A PROOF-OF-CONCEPT FOR THE IMPLEMENTATION OF A EUROPEAN COPERNICUS COASTAL FLOOD AWARENESS SYSTEM

www.ecfas.eu

Report on the intercomparison between CMEMS and ANYEU-SSL modelling systems

Deliverable No.: D4.2 – Intercomparison between CMEMS and ANYEU-SSL modelling systems

Ref.: WP4 – T4.4 –D4.2

This project has received funding from the Horizon 2020 research and innovation programme under grant agreement No. 101004211

Document information

Deliverable	D4.2 - Report on intercomparison between CMEMS and ANYEU-SSL modelling systems
Reference	WP4 – T4.4 –D4.2 Report on the intercomparison between CMEMS and ANYEU-SSL modelling systems
File name	D4.2_ECFAS_Deliverables.pdf
Editor(s)	Melet, Angélique (MOi) Ciavola, Paolo (CFR) Fernàndez-Montblanc, Tomàs (UCA)
Author(s)	Irazoqui, Maialen (MOi) Le Gal, Marine (CFR) Fernàndez-Montblanc, Tomàs (UCA) Melet, Angélique (MOi) Ciavola, Paolo (CFR)
Contributor(s)	
Dissemination level	PU – Public
Date	28/06/2022
How to cite this document:	Irazoqui M., Le Gal M., Fernàndez-Montblanc T., Melet A., Ciavola P., 2022. Report on the intercomparison between CMEMS and ANYEU-SSL modelling systems. Deliverable 4.2 - ECFAS project (GA 101004211), www.ecfas.eu

Document history

Version	Date	Leading editor/author	Reviewed by
1.0	20/05/2022	Irazoqui, Maialen (MOi)	Pujol, Isabelle (CLS)
1.1	23/06/2022	Irazoqui, Maialen (MOi)	Armaroli, Clara (IUSS)
2.0	28/06/2022	Le Gal, Marine (CFR)	

Summary

The present work aimed to identify the required level of complexity in numerical models for the accurate representation of coastal water-levels used as marine forcing in coastal flood warning applications such as ECFAS. The level of complexity is evaluated in terms of added physical processes as well as the 2-dimensional (2D) or 3-dimensional (3D) nature of the models. To this aim, the model systems used in ECFAS to produce hindcasts - ANYEU-SSL (2D) - and forecasts - CMEMS (3D), for the IBI region were tested. Two added physical processes were considered: the surge and tide non-linear interaction and the wave and surge non-linear interaction. The inclusion of these processes is tested by activating tidal propagation (tested in ANYEU-SSL only) and by accounting for wave effects in the baseline ocean circulation models, respectively. Adding the tidal forcing in the ANYEU-SSL notably affected storm surge simulations, especially in the North Western Shelf (NWS) and during extreme conditions, confirming its utmost importance. Concerning the inclusion of the wave-surge non-linear interaction, the CMEMS-IBI (3D) model is tested for the incremental inclusion of the Stoke-Coriolis effects, the wave induced modification of the momentum flux to the ocean (including sea-state dependent roughness) and wave induced mixing, while ANYEU-SSL (2D) integrates only the sea roughness and radiation wave stress. The two models differ on multiple aspects, such as their baroclinic or barotropic configurations, bathymetry and its caping, the grid resolution, and atmospheric forcings, allowing only a qualitative comparison. Largest impacts of the wave-surge non-linear interactions are seen during extreme conditions and in the NWS region for both CMEMS-IBI and ANYEU-SSL models. While the wave-surge coupling impact significantly affected model surge magnitudes (with impacts of up to 30%) for CMEMS-IBI giving a great improvement in the predictive skill (+50%) and matching the literature, the impact measured with the ANYEU-SSL model is much less (10-15%) with an improvement of skills of only 2% (while larger locally). This difference of scale in the impact is probably due to the numerous model differences, including wind stress parameterisation. The ANYEU-SSL experiments do not allow strong conclusions regarding the benefits of wave-coupling and a deeper and more specific analysis would be beneficial. Nonetheless, given these results and the associated relevant literature, the inclusion of both tide-surge and wave-surge interactions are recommended for future evolutions of the ECFAS system, as currently all/some of these processes are missing in the hindcast/forecast products used within the current ECFAS proof of concept. In view of this, an increased coherence between the forecast and hindcast TWL datasets is recommended to guarantee the appropriate and timely triggering of the ECFAS system.

Table of Contents

List of Figures

List of Tables

List of Main Acronyms

C3S	Copernicus Climate Change Service
CEMS	Copernicus Emergency Management Service
CLMS	Copernicus Land Monitoring Service
CMEMS	Copernicus Marine Environment Monitoring Service
DIAS	Data and Information Access Services
ECMWF	European Centre for Medium-Range Weather Forecasts
EFAS	European Flood Awareness System
EO	Earth Observation
ESA	European Space Agency
EU	European Union
H2020	Horizon 2020 programme
LRA	Local and Regional Authority
LU/LC	Land Use / Land Cover
MED	Mediterranean
NWS	Northwest Shelf
NTR	Non-tidal residual or surge
PoC	Proof-of-Concept
RM	Rapid Mapping
RMSE	Root Mean Squared Error
RRM	Risk and Recovery Mapping
SDS	Satellite Derived Shoreline
SSL	Storm Surge Level
TWL	Total Water Level
WL	Water Level
WP	Work Package
2D(H)	2-dimentional/depth averaged
3D	3-dimensional

1 Introduction

1.1 The ECFAS project in brief

The ECFAS project aims at demonstrating the technical and operational feasibility of a European Coastal Flood Awareness System, which is a candidate for the evolution of the Copernicus Emergency Management Service (CEMS). ECFAS capitalises on Copernicus core services product portfolios and on the existing CEMS-EFAS (European Flood Awareness System) framework. ECFAS will provide a proof-of concept (PoC) that will complement and broaden the currently available panoply of core service information. ECFAS will tackle coastal resilience to climate risk (marine storminess) and population exposure risk (e.g. in coastal areas prone to flooding). ECFAS will contribute to a fully integrated risk cycle monitoring service, through the implementation of an awareness system specifically targeted to coastal areas (preparedness phase) and impact assessment (response phase) in the aftermath of a flood event, playing a fundamental role for the implementation of effective recovery and prevention actions. Following the principles of subsidiarity and proportionality, the avoidance of duplication, and the facilitation of user uptake, ECFAS capitalises from the products portfolio of the Copernicus Emergency Management, Marine and Land Monitoring Services (CEMS, CMEMS and CLMS), also using other publicly available datasets and information derived from past and ongoing initiatives and relevant FP7 and H2020 EU projects. Marine forcing forecasts from CMEMS are validated at pan-European level using hindcasting of past events, to reduce uncertainties and provide reliable forcing datasets to compute inland inundation extension, water depth and velocities with the numerical model already implemented in EFAS (LISFLOOD-FP). Impact assessment is carried out taking into account the existing CEMS framework, producing a set of added value components for the Rapid Mapping and Risk and Recovery products. The technical operational feasibility of the products will be demonstrated through the implementation of the full operational chain, from the forecasting to the impact assessment component. A performance assessment of the service in hindcasting mode at selected test cases, as well as in forecasting mode during the duration of the project, will be carried out. The Technology Readiness Level for a full Copernicus operational deployment in the future at pan-EU level will be evaluated, as well as the feasibility, calendar and cost benefits of the developed products for inclusion. A Roadmap for the operationalisation of the system will be delivered at the end of the project. The integration of data from different sources will require increased computer resources ensured by the usage of the Data and Information Access Services (DIAS) as core

processing and databasing service. Additionally, in order to improve and strengthen the strategies implemented in previous experiences (e.g., GREEN, CLARA EU projects) a standardized methodology to collect, analyse and prioritize the user needs and, successively, identify the service requirements will be defined. The ECFAS concept is summarized in Figure 1.1.

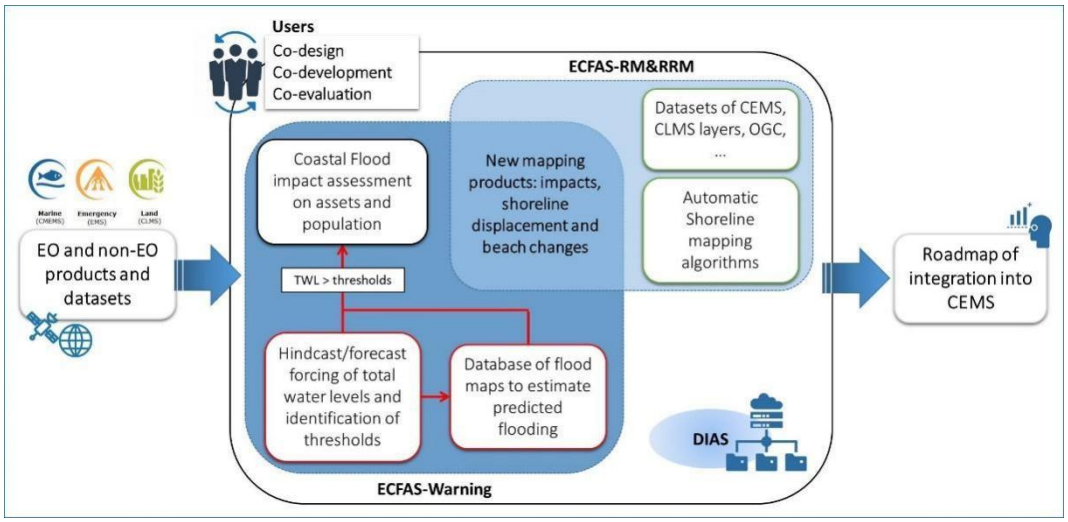

Figure 1.1 The ECFAS concept.

1.1.1 Objectives

ECFAS main objective is to develop products and tools for the evolution of the Copernicus Emergency Service (CEMS hereafter) in the coastal area. ECFAS will demonstrate the technical operational feasibility of one specific application of CEMS that will be relevant for the enhancement of Copernicus core services and will capitalise from the corresponding product portfolio. ECFAS will provide a proof-of-concept (PoC) that will complement and broaden the currently available panoply of core service information to contribute to the evolution of Copernicus services.

ECFAS will provide and demonstrate tools, methods, and protocols that will focus on the implementation of a coastal flood awareness system using the European Sentinel Series EO data, complemented by the integration of previous EO missions (e.g., Landsat) and Contributing Missions, in conjunction with oceanographic modelling, high resolution LU/LC mapping of the coastal area, location and characteristics of exposed assets, including the population, and numerical modelling of coastal floods. Shoreline displacement evaluation will allow the assessment of the impact of marine storms and consequent flooding of the hinterland, enhancing rapid mapping products and Risk and Recovery Mapping services of

CEMS, adding coast-targeted products. Services C3S, CEMS, CLMS and CMEMS will guarantee the provision of products derived from Sentinel data as well marine modelling products. These will be integrated with third-party data (including in-situ data) and assimilated into models available on the Copernicus services platform and by previous EU projects.

ECFAS will operate at different levels to provide an integrated risk management service. A first component (ECFAS-Warning) is related to the improvement of EFAS (European Flood Awareness System) to build an awareness system for coastal areas, following the framework and technical requirements of EFAS, to guarantee its full integration. A second component (ECFAS-Rapid and Risk and Recovery Mapping, ECFAS-RM&RRM) will provide added-value products to improve the Rapid Mapping. ECFAS will improve marine forcing hindcasting and forecasting through the integration of existing data and models of CMEMS with the ANYEU-SSL (Fernandez-Montblanc et al., 2019) model developed in the EU H2020 ANYWHERE project and identify marine forcing thresholds able to trigger coastal flooding.

1.1.2 Structure

WP1 is devoted to coordination and management of ECFAS and will assure smooth progression and effective achievement of project results, facilitating communication among the partners.

In WP2 users' requirements will be identified together with the regulatory framework, including relevant international Conventions and EU Directives, throughout the whole project duration. Users' engagement will be stimulated involving the national coordinators of the Copernicus User Forum and national delegates at the Copernicus EU User Forum in order to reach a larger audience.

WP3 will identify the available datasets of exposure and vulnerability components of the coastal zone and will select the "optimal" algorithm to extract the Satellite Derived Shoreline. The algorithm will be used in WP5 and integrated in the platform in WP6.

WP4 will provide pan-European hindcasts and up to 5-day forecasts of total water levels at the coast, including contributions from tides, waves, storm surges and dynamic sea level including steric sea level effects related to ocean circulation and density fields. Different modelling systems will be used to produce TWL. A joint analysis of simulated TWL and past coastal flooding events will allow identifying local thresholds of TWL for which coastal flooding could occur and that will activate coastal flood mapping (WP5).

WP5 represents the integration of the products defined in WP3 and WP4 into the operational chain of the awareness system. The WP5 phases will follow a specific set of activities: (i) identification of test sites; (ii) calibration and validation of the flood model (LISFLOOD-FP) at test sites; (iii) implementation of the "mapping" module of the system on the basis of the products already provided in CEMS; (iv) implementation of the impact assessment on assets, population, etc. including a coast-targeted product; (v) system performance evaluation in hindcast and forecast mode at pan-EU level.

WP6 is dedicated to the design of the proof-of-concept and its integration into existing core services in accordance with the requirements relevant to the needs of the users as defined in WP2. The products of the different phases of the PoC implementation will be operationally tested by users to ensure sustainability of the development through co-design, co-development and co-evaluation methodologies.

WP7 will deal with communication, dissemination, exploitation and uptake, including IPRs. It will include the dissemination of the results of the project to different types of audience: private, institutional and academic users, a wide stakeholder audience (comprising industry and policy makers, civil protection, coastal managers and disaster risk reduction professionals). It will also deal with the Exploitation Plan to identify project's outputs with a potential for exploitation and by addressing dissemination issues and strategy.

The WPs structure and connections are represented in Figure 1.2.

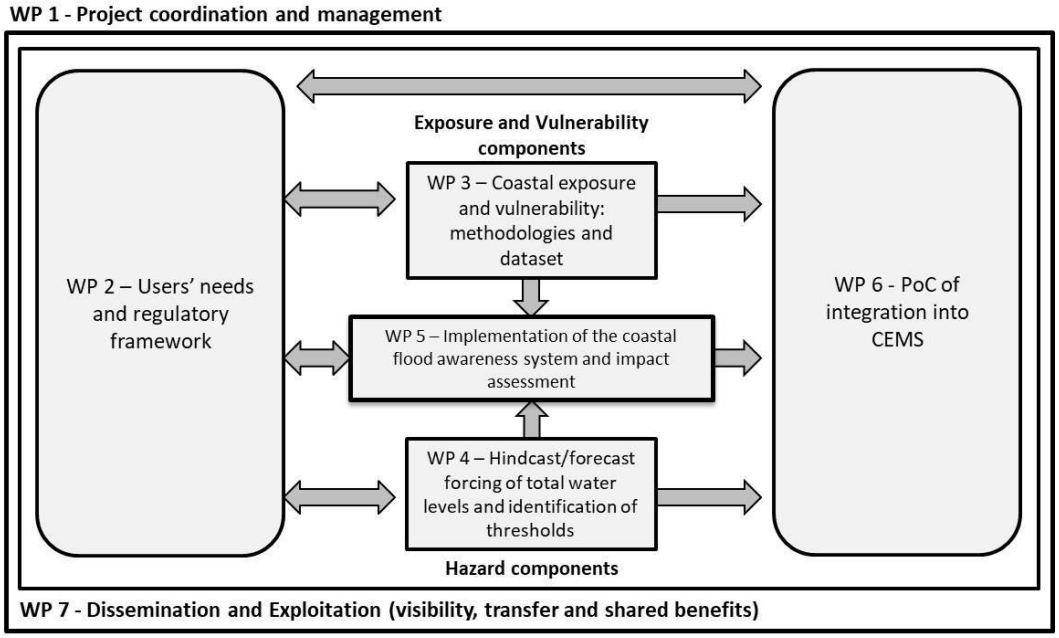

Figure 1.2 Structure of the project.

1.2 Context and objectives of the document

In the context of coastal water-level (WL) forecasting for coastal flood risk applications, depth-averaged models are often used (2DH hereinafter) whereby the water-levels are reduced to the effects of tides and sea-level variations induced by surface winds and atmospheric pressure, commonly denoted as surge. These WL variations are commonly known as 'barotropic motions'. However, in reality the WL is additionally composed by the effects of ocean circulations and steric effects (due to density changes), commonly known as 'baroclinic motions'. In this regard, 3-dimensional ocean models (3D hereinafter) are needed to resolve the combined effect of baroclinic and barotropic processes on the WL. The 3D vs 2DH nature of models has therefore implications on their capability to represent WLs, both directly due to the nature of the motions they can describe and indirectly due to, for example, differences in the representation of the ocean surface fluxes with the atmosphere as well as the interaction with waves. The preferred use of 2DH models is generally stemming from the significantly lower computational cost of 2DH models compared to 3D models, which facilitates applications such as ensemble forecasting. Additionally, 2DH models result in simpler model development and calibration, which can be easier targeted than for the physically more complex 3D models. Beyond the 3D and 2DH nature of a hydrodynamic model, additional physical processes that influence the WLs may be included. Some of the most important

include the non-linear tide and surge interaction and the coupling with waves. Existing Early Warning Systems that target coastal flood risk at regional to continental scales present varying levels of complexity related to the aforementioned modelling options. As such, the question arises: what is the impact of the degree of (physical) complexity of numerical models on the accuracy of the produced TWL that feed coastal flood risk applications, and what is the relative importance of each physical process?

Within the ECFAS system, hydrodynamic models of different complexity are used for different components of the system (see **D4.1 – Report on the calibration and validation of hindcasts and forecasts of TWL**). 3D-ocean models from the Copernicus Marine Service are used to produce daily 5-day forecasts of TWL, predicting upcoming and potentially threatening marine-storm events. In turn, a 2DH model called ANYEU-SSL is used for past TWL reconstructions (hindcast) through linear combination of the ANYEU-SSL surge component, the FES2014 tides (Lyard et al., 2021) and the Copernicus Marine Service global model reanalysis mean sea level variations, and is used to produce the historical flood catalogue (**D5.4 -Pan-EU flood maps catalogue**). As such, these models are used in the present task **(T4.4 - Intercomparison of CMEMS and ANYEU-SSL models to identify optimal settings and to provide recommendations for TWL forecasting systems)** to explore the effects of the different degrees of model complexity on TWLs, with a focus on extremes, with the objective to provide recommendations for the next generation of TWL forecasting systems (**D6.4 - Roadmap of ECFAS integration into CEMS**). Additionally, the inter-model comparison between the 2 systems will allow for a better understanding of their possible biases and related impacts at the triggering stage of the warning component of the system.

1.3 Approach

The evaluation of the impacts of different levels of model complexity on TWLs is done in two steps. First, the impact is evaluated within each modelling system – ANYEU-SSL and CMEMS-IBI models - where the model complexity (and in principle realism) is increased gradually in a set of experiments by including additional physical processes (intra-model comparison). The physical processes evaluated are the effects of non-linear tide and surge interaction, which is only evaluated within the 2DH ANYEU-SSL model; and the effects of ocean-wave coupling, which is evaluated for both systems. Second, the identified intra-model sensitivities are compared between the two systems (inter-model comparison). Additionally, comparisons to coastal tide-gauges from the Copernicus Marine Service are performed in order to evaluate the

impact of the additional complexity on the model performance for each modelling system. Further details on the approach and methods can be found in section 2.

1.4 Outline of the document

The report is organized as follows: section 2 describes in detail the modelling systems and methods used to quantify the intra-model sensitivities to added physical complexity. Section 3 shows the results of such intra-model comparison. Section 4 is dedicated to the inter-model sensitivity assessment. Section 5 provides a discussion of the results from previous sections, including benchmarking against existing literature. Section 6 informs on the impacts of the present results for the ECFAS evolution and roadmap. Finally, section 7 provides the summary of the findings and the conclusions derived.

2 Description of the models and methods

2.1 CMEMS-IBI model

The CMEMS-IBI model is a 3D ocean model based on the NEMO modelling suite (version v3.6, Madec et al., 2017). It corresponds to a former release of the operational system currently operated within the Copernicus Marine Service (CMEMS, https://marine.copernicus.eu/). The model is used in the present work at its native grid, covering the European Northwest Shelf, Iberian Biscay, Irish Sea, and Western Mediterranean. The model has 50 vertical layers, and the spatial resolution is 1/36 degrees (2-3km) which is uniform across the domain. The bathymetry is based on the 30-seconds GEBCO08 dataset plus local datasets. For tidal forcing, the model is forced at the open boundaries with 11 tidal constituents (M2, S2, N2, K1, O1, Q1, M4, K2, P1, Mf, Mm) from the FES2014 solution (Lyard et al., 2021). Additionally, the model is forced by its parent ocean model, the global CMEMS-GLOBAL system (product identifier GLOBAL_ANALYSIS_FORECAST_PHY_001_024). The model is forced with river forcing from NRT-gauges when available, and the E-HYPE climatology database otherwise. The model includes the assimilation of sea-level anomaly from altimetry. For meteorological forcing, the model uses hourly surface forcing from the ECMWF IFS HRES operational dataset (documentation: https://www.ecmwf.int/en/forecasts/documentation-and-support), with a 1/12-degree resolution. For further information on the CMEMS-IBI operational model, the reader is referred to the Product User Manual (PUM) and the Quality Information Document (QUID) published in the Copernicus Marine Service alongside the dataset (product identifier IBI_ANALYSISFORECAST_PHY_005_001).The wave model used for coupling corresponds to the operational wave CMEMS model counterpart for the IBI region (IBI_ANALYSIS_FORECAST_WAV_005_005), based on the MF-WAM code (e.g. Aouf et Lefevre, 2015). The model has a spatially uniform 5km resolution, it is consistently forced by the ECMWF-IFS HRES winds, and it assimilates significant wave height from altimetry. For more information, the reader is referred to the corresponding Product User Manual (PUM) and the Quality Information Document (QUID).

For the present work, the following coupling processes from wave to ocean are implemented: the effect of the Stokes-Coriolis drift, the combined effect of the modification of the ocean surface roughness by the wave state and the absorption and release of momentum by the waves during growth and dissipation respectively (denoted as ‘momentum flux modification’), and the wave-breaking induced vertical mixing (denoted as ‘energy flux modification’). For a

detailed explanation of each process and the corresponding parameterization the reader is referred to Law Chune & Aouf (2018). It is noteworthy that the coupling takes places in a one-way, offline fashion, meaning the waves that are coupled to the ocean haven't seen the ocean first. This poses certain limitations to the accounting of coupling effects between the two systems.

Table 2.1.1 shows the experiments performed for the assessment of wave-coupling impacts in the CMEMS-IBI model. As shown, the level of coupling is gradually increased from a non-coupled reference run to a fully coupled configuration.

Table 2.1 Model experiments performed for the assessment of wave-coupling impacts in the CMEMS-IBI model.

Simulation period	Experiment ID	Stokes-Coriolis	Momentum flux modification	Energy flux modification
2018	control	x	x	x
2018	stokes	✓	x	x
2018	tauoc	✓	✓	x
2018	cb (Fully coupled)	✓	✓	✓

2.2 ANYEU-SSL model

The ANYEU-SSL model, an upgraded version (see **D4.1 – Report on the calibration and validation of hindcasts and forecasts of TWL**) of the model in Fernández-Montblanc et al. (2019, 2020) was implemented at pan-European scale using the SCHISM model (Semi-implicit Cross-scale Hydroscience Integrated System Model), based on the original SELFE code (v3.1dc, Zhang & Baptista, 2008). SCHISM is two-way coupled with the spectral wave model WWM III (Wind Wave Model III), a spectral wave model developed by (Hsu et al., 2005) and updated by (Roland et al., 2012). The model resolution is 2.5 km along the European coastline; the friction coefficient spatially varies in the 2D domain; providing hourly outputs. The circulation model was forced at the boundary with the main 12 tidal components (SSA, SA, M2, S2, N2, K2, K1, O1, Q1, P1, MM, MF) obtained from FES2014 (Lyard et al., 2021) and tidal forcing. The regional WWMIII wave model was forced at its ocean boundary with parametric time series of waves from the ERA5 reanalysis (Hersbach et al., 2020) . The atmospheric forcing variables used were the wind speed at 10-m height (u10, v10) and mean sea level pressure (m.s.l.p) from the ERA5 reanalysis.

Information on the circulation and wave model coupling are detailed in Roland et al. (2012) . For the present work, 6 models, called hereafter experiments, were produced with different configurations between surge, tide, and wave configuration for the year 2018. The characteristics of each experiment are summarised in Table 2.1.2. Two incremental settings can be chosen. With the half-coupled model (one way), the wind stress component of the circulation model, initially estimated with the Pond & Pickard (1983) formulation, is updated by integrating the sea roughness from the wave model. With the fully-coupled model (two-way coupling), in addition the wave radiation stress is shared from the wave to the circulation model and the water level and currents are updated in the wave model from the circulation model. It is important to note that while E5 and E4 do not include tides, E3 and E2 do (Table 2.1.2), leading to possible interactions between the wave and tide. This interaction is not assessed in this exercise.

Table 2.2 ANYEU-SSL's experiment considered for this exercise with its different settings.

Simulation period	Experiment ID	SSL	tide	wave
2018	E2	✓	✓	x
2018	E3	✓	✓	✓ Fully coupled
2018	E4	✓	x	✓ Non coupled
2018	E5	✓	x	✓ Half-coupled
2018	E6	x	✓	x

The model E4 is used as control for this analysis as the resulting surge is not subjected to any interaction with tide or wave. For assessing the wave-surge interaction and the influence of the level of wave coupling (none/ half/ full), E5 and E3 are compared to E4 and E2, respectively. For assessing the impact of the tide-surge non-linear interaction, the water level in E2 is compared to a new water level variable created by linearly adding the tide from E6 with the surge from E4. For comparison of the surge signal, which is obtained as the non-tidal residual of the water level, the water level is de-tided using the Utide package (Codiga, 2011), see section Method and metrics.

2.3 Method and metrics

In order to evaluate the relative importance of the stated physical processes on the representation of (extreme) coastal total water-levels, metrics are computed for the model

output at the coastal points. A visual comparison of the coastline as defined by each model revealed that models generally agree on the location of the coastline other than in certain regions characterized by the presence of salt-water coastal lagoons, large estuaries, and shallow-water island locations such as the Wadden Islands. In order to guarantee a fair comparison, a set of common coastal points was defined between the two models.

To compare the result between the models and observation data, two kinds of metrics are used: yearly and extreme event metrics. The yearly metrics represent the annual variability of the considered variable (water – level or Non-Tidal Residual, NTR) at each point during the full year 2018. The centred Root Mean Square Error (RMSE) and the normalised RMSE_NG are defined such as:

$$RMSE = \sqrt{\frac{\sum_1^n (x - x_{ref})^2}{n}} \text{ and } RMSE\_NG = \frac{RMSE}{\sqrt{\frac{\sum x_{ref}^2}{n}}},$$

Where x and x_{ref} are the variables for the tested and reference model, respectively; n is the number of points in time. During extreme events, which is the main focus of the ECFAS system, the metrics used for evaluating the difference between the models are the absolute and relative peak difference during a given storm event:

$$diffPeak = peak_{ref} - peak \text{ and } diffPeak_{rel} = \frac{diffPeak}{peak_{ref}}.$$

To identify the extreme events within 2018 and compute these indicators, a peak over threshold method is applied using the percentile 99 for the surge and 99.9 for the water level and a 3-day meteorological independence criteria to separate extreme events (**D4.1 – Report on the calibration and validation of hindcasts and forecasts of TWL**). Note that, given the short period at hand (1 year), it is decided to focus on the meteorologically driven part of the water-level (i.e., the surge or non-tidal residual, NTR) to increase the sampling of storm-driven events. It is also in this component where one expects to see the strongest impact of the evaluated physical processes. As such, much of the results in sections 3 and 4 focus on the impacts on the surge or NTR. To separate the water-level into its tidal and NTR components, the UTIde package was applied based on harmonic analysis (Codiga, 2011) .

As previously mentioned, the impact of the additional processes is evaluated by assessing the relative changes induced by them within the model, allowing for an evaluation at every model coastal cell. Additionally, the impact of the additional processes in the model skill is also

evaluated through comparison against tide-gauge data. While TG data may be somewhat sparse, this gives the opportunity to compare all model experiments to a common truth. The tide-gauge data corresponds to that of the Copernic Marine System, and the data processing was thoroughly described in **D4.1 – Report on the calibration and validation of hindcasts and forecasts of TWL** and therefore omitted here. Similarly, the tools to compute the aforementioned (skill) metrics were developed in the validation activities within **T4.1 Forecasts of total water levels** and adapted to accommodate a model-to-model comparison.

3 Model intra-comparison

3.1 ANYEU-SSL model

3.1.1 Nonlinear tide-surge interaction

The impact of the nonlinear tide-surge interaction is assessed by comparing the components of the total water level resulting from the linear addition of the surge of the experiment E4 and the non-coupled tide from the model E6 to that of the experiment E2. Both total water levels were de-tided to compare separately surge and tide components. First, the impact on the average conditions is evaluated by looking at the yearly difference (RMSE and RMSE_NG) between the two experiments. As shown by Figure 3.1.

, the inclusion of the tidal processes in the simulation clearly impacts the surge results especially in the North-western Shelf (NWS). In average, a 12 cm difference is detected in the NWS and slightly smaller changes along the English Channel. The Bristol Channel stands out with a maximal RMSE of 20cm. Looking at the normalized metrics (panels c,d in Figure 3.1), the impact appears more widespread across the NWS, with the Southern coast of England, the Bristol Channel and the southern Irish Sea showing strong impacts (more than 40%). The normalized results highlight also some micro-tidal areas such as the eastern part of the Black Sea and the Baltic Sea with around 20% of change. This is equivalent to 2-3 cm in the Baltics and around 1 cm in the Black Sea.. In the Mediterranean, areas with shallower depth also seems to be relatively impacted such as the Gulf of Gabes (more than 20 % of average change) and to a lesser extent (around 15-20 % of average change) the North Adriatic Sea.

On the other side, the tide is slightly affected, only a few centimetres (less than 5%) in the NWS with still a peak at the Bristol Channel of about 22cm. Significant normalized tidal changes emerge in the micro-tidal areas (between 30 and 40 % in Baltic Sea and around 20 % in the Black Sea) and in the Danish straits (more than 40%).

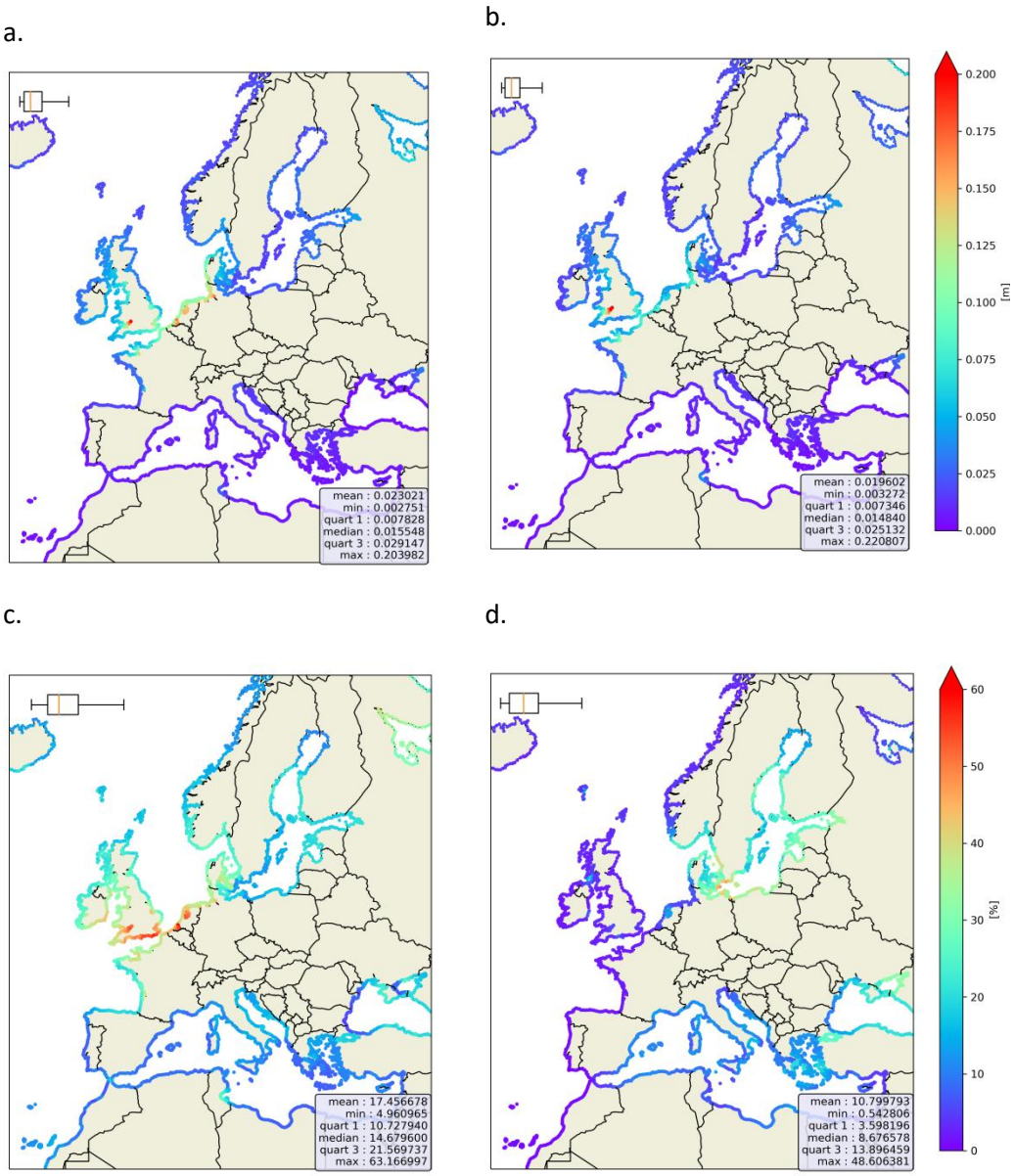

Figure 3.1 Impact of the tide - surge interaction on average conditions, measured as the RMS of the difference (RMSE) between signals. a. and b. show the metric for surge and tide respectively [m], while c. and d. show the normalised metric RMSE_NG.

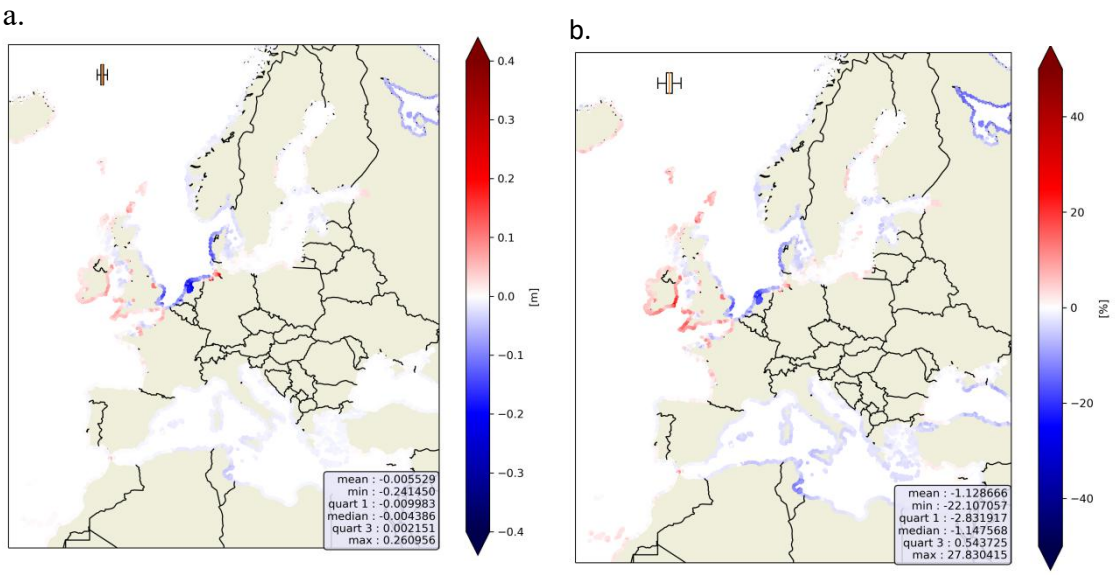

Figure 3.2 a. Absolute and b. relative surge peak magnitude difference between the linear addition of tide and surge-only simulations (E4+E6) and the tide-surge coupled model (E2) during extreme events. The red colour indicates an increase of the surge peak magnitude while the blue colour a decrease when adding the tidal coupling.

Focusing on the extreme events, only the impact on the surge has been assessed through the difference in the average peak magnitudes across the detected extreme events. The interaction between the tide and surge is more important than for yearly average conditions, see Figure 3.2. The peak surge is increased (maximum of 27%) around Ireland, Bay of Biscay, Cornwall (UK) and for most of the coasts around the English Channel, while it is decreased around the Mediterranean Sea and the North Sea by a minimum of -22%. Important increases are witnessed in bays and estuaries such as the Bristol Channel, the Elbe Estuary and the Mont Saint-Michel Bay. These areas are characterised by strong tidal amplitudes and shallow depths.

Timeseries for the year 2018 in these particular areas are gathered in Figure 3.3 , with a focus on the impacts during extremes (peak surges). At Hoek Van Holland (Dutch coast) the biggest difference between the model's peaks is obtained during the stormy seasons, i.e., between October and March for which we can expect higher value of the surge, and thus bigger interactions between the processes. However, differences between the two models are visible all year long with a RMSE of 11cm. In average the tidally-coupled model (blue markers) shows smaller peaks than the non-tidal model as highlighted previously on Figure 3.2.

When focusing on the storm Eleanor (early January 2018) which was the biggest surge event of the year, the tidally-coupled model gave a narrower signal with a maximal peak earlier than the non-tidal model. Contrary to the rest of the year, for this event the amplitude of both peaks is similar. At the Elbe Estuary, see Figure 3.3-b, again the main deviation occurs between

November and March, in the period of more important surge events. However, in this case, the tidally-coupled model gives similar to higher surge peaks than the non-tidal model as shown in the spatial plots in Figure 3.2. The RMSE between the two timeseries is about 18 cm for the entire year. During the Eleanor storm, the tidal model gives again a narrower surge signal with a 1 m higher peak amplitude. Eventually, the timeseries extracted from both models at Port Ferreol (France, Mediterranean coast) are displayed in Figure 3.3-c, showing minor differences (RMSE = 1 cm) as it could be expected in such a micro-tidal area.

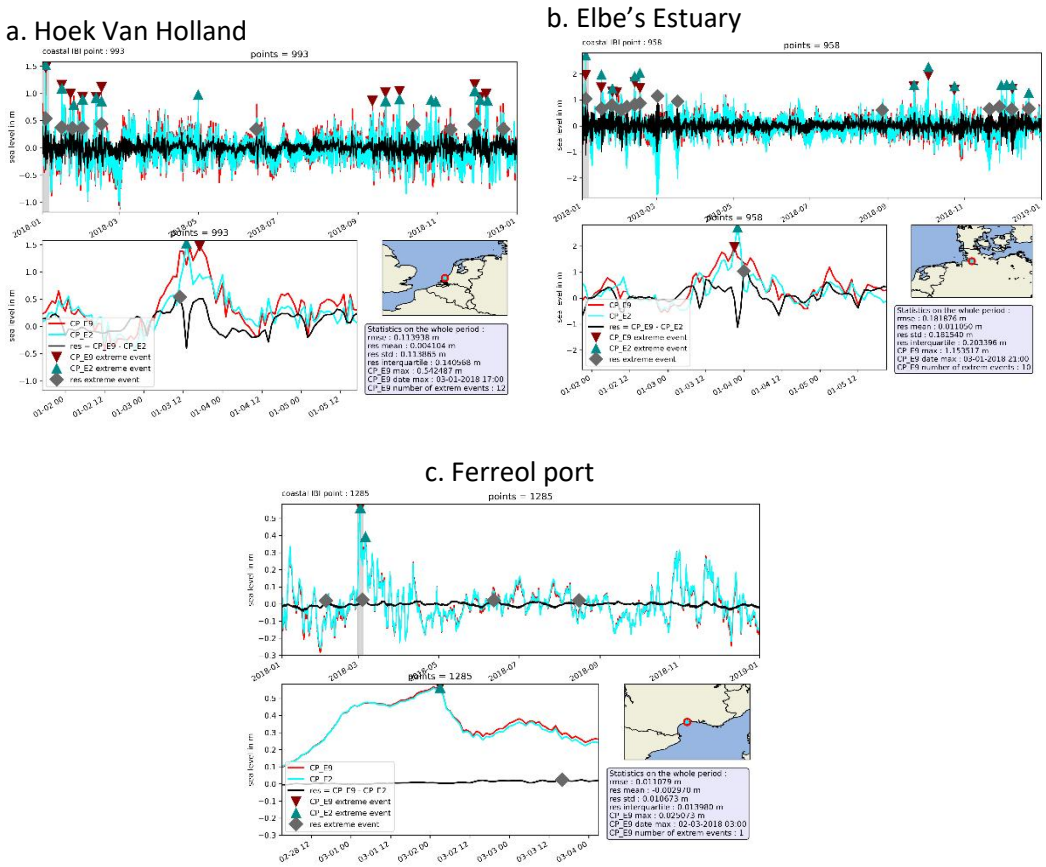

Figure 3.3 Timeseries extracted from the linear addition of tide and surge-only simulations (E9=E4+E6, red curve), the tide-surge coupled model (E2, blue curve) and their difference (black curve) at a. Hoek Van Holland, b. Elbe Estuary and c. Port Ferreol. The triangle markers indicate the peak magnitude for the detected extreme events by peak above the 99th percentile. The captioned graph shows a zoom on the extreme event of the year with the greatest peak magnitude.

3.1.2 Wave coupling effects

In this section the impact of the inclusion of the wave coupling process on the surge is assessed. The impacts of the sea roughness integration are measured by comparing the half-coupled model (E5) to the non-coupled surge (E4), while the impact of full wave-surge coupling is assessed through the comparison of the fully coupled model (E3) to the non-wave coupled

model (E2).

Similarly, to the tide-surge interaction evaluation, metrics for yearly average and extreme conditions are evaluated.

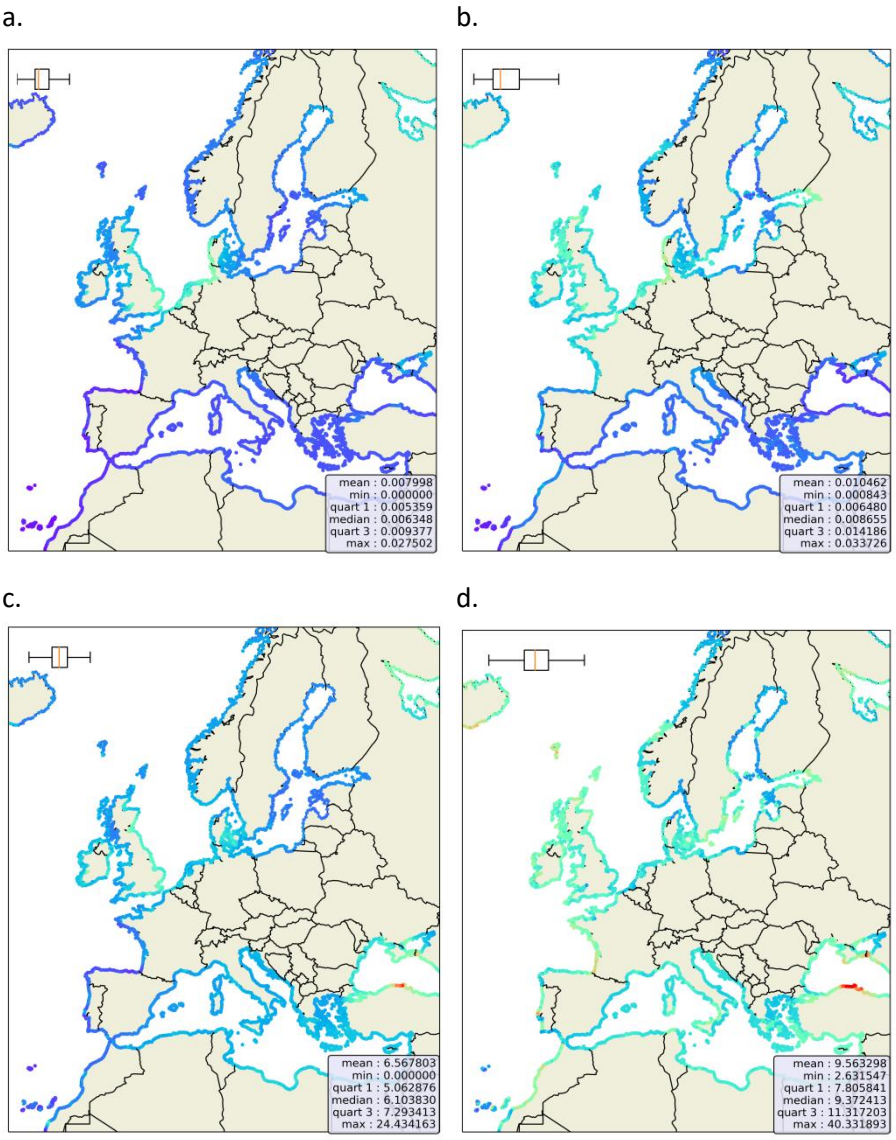

Figure 3.4 Yearly impact of the wave - surge interaction. The top row shows the RMSE estimated for a. the half coupled wave model and b. the fully wave coupled model. The second row is the relative RMSE for c. the half coupled model and d. the fully coupled model.

Looking at yearly average metrics in Figure 3.4, both half-coupled and fully coupled model have an influence on the resulting surge.

For the half-coupled model (panel a), the effect focuses on the North-western shelf (NWS) with a maximum of 2.7 cm of difference from the control surge while it is negligible in average throughout Europe (mean RMSE = 7 mm). On the normalised result, in addition to the NWS for

which the surge varies of around 12%, the Eastern Mediterranean is also prominent and in particular the Black Sea. Supposedly, this could be resulting from the small surge in these areas (around 8 cm in the Eastern Mediterranean and 5 cm in the Black Sea), amplifying the normalisation effect. In average, the normalized impact is of 6%.
For the fully coupled model, the average change is about 1 cm throughout Europe with highest values on the German Bight (maximum at 3.3cm). In addition, the additional coupling affects the Irish Sea area, the French Atlantic coasts, and the Eastern Baltic Sea areas. When normalising this result, the whole European area appears sensitive to the wave coupling, with a 9% change in average, and strong normalized impacts in the Bay of Biscay, Peniche - Portugal (15%) and the southern part of the Black Sea (40%). For the latter, it could be due again to initially small surges in this area. In contrast, the relative effect of this additional wave coupling settings seem weaker on the North Sea, which appears dominated by the effect of the sea-state dependent sea-surface roughness

During extreme events, see Figure 3.5, both half and fully wave-coupled models show a similar duality in the trend between northern and southern European coasts: a decrease of the extreme storm surges on the Mediterranean Sea, South Atlantic area and eastern Black Sea coast while an increase of the surge peak in the North Atlantic, North-West shelf, Baltic Sea and western Black Sea coast. By comparing the trend between the two wave-coupling settings, except for the North Moroccan Atlantic coast and the Shetland islands (North of Scotland), the fully coupled setting seems to intensify the impacts seen for the inclusion of the sea-state dependent sea roughness effect. For example, a clearly intensified decrease of extreme surges is seen along the Mediterranean coast, while a further increase of extreme surges is observed on the German bight. On the fully coupled model, the area of Cadiz (Southern Spain) shows an increase of the surge peak not seen for the half-coupled simulation. Looking more closely to the timeseries at Huelva (around 100 km away) on Figure 3.6-a, one can see that this difference appears mainly during the Emma storm that hit the coast beginning of March 2018. At this occasion, including the wave – surge interaction enhanced the storm surge peak by less than a centimetre with a yearly RMSE of 4 mm. This is smaller than expected from Figure 3.6-b, showing the importance of the local environment. At Hoek Van Holland (Dutch coast), the fully wave- coupled model gives very similar result that the non-coupled model with a yearly RMSE of 1 cm, with only slight differences appearing during extreme events, such as the Eleanor storm. On Mediterranean coast, looking at the timeseries at Sète (South France) a more consistence decrease of the surge seems to take place all year long (RMSE close to 1cm) with a

slight increase of the difference during the extreme events as illustrated by the event of the 1st of March 2018 (storm Emma).

a. b.

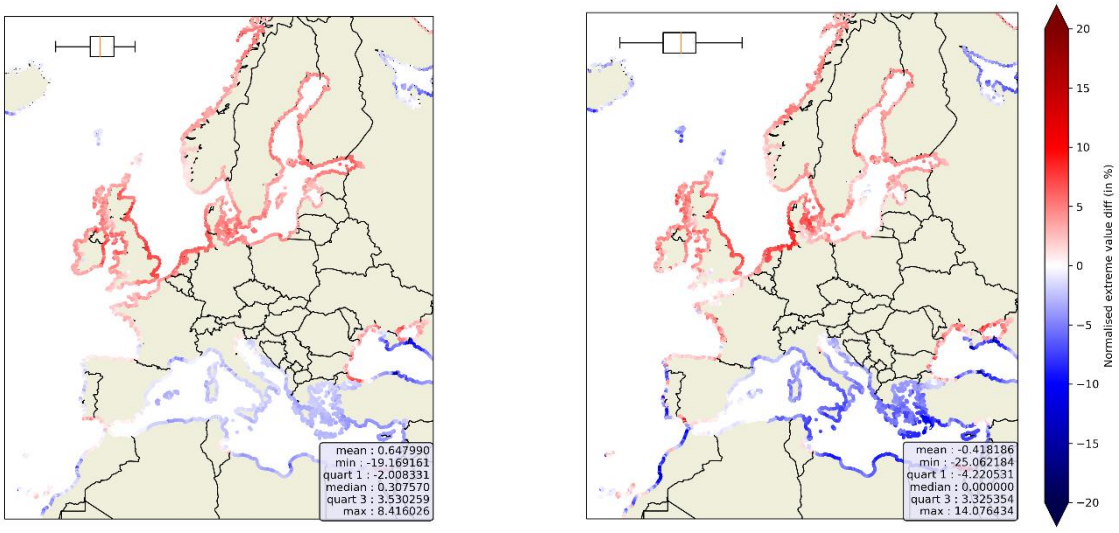

Figure 3.5 Normalized surge peak magnitude difference for a. the wave half-coupled (E5 vs E4), b. the wave fully coupled (E3 vs E2) experiments.

a. Huelva b. Van Hoek Holland

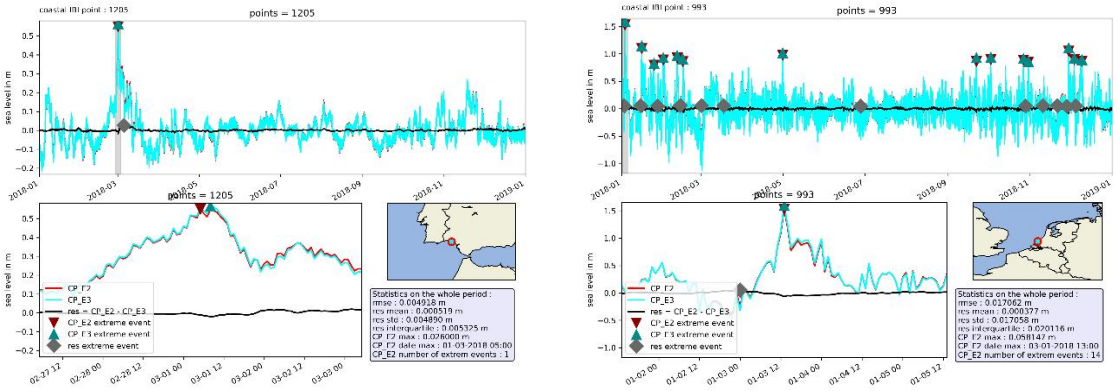

c. Sète

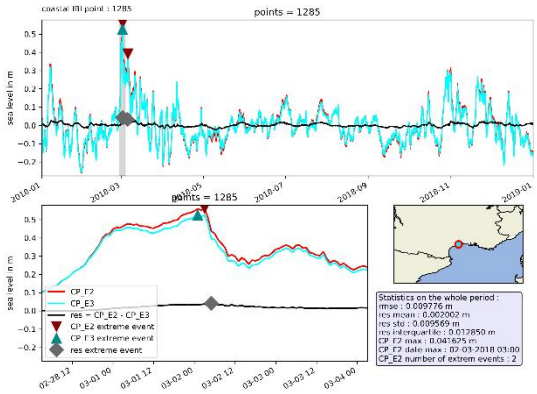

Figure 3.6 Timeseries extracted from the control non-wave model (E2, red curve), the fully wave coupled model (E3, blue curve) and their difference (black curve) at a. Huelva, b. Hoek Van Holland and c. Sète. The triangle markers indicate the peak magnitude for the detected extreme events. The captioned graph shows a zoom on the extreme event of the year with the highest peak magnitude.

3.1.3 Impact on model performance

In this section, the impact of the wave coupling inclusion on the model performance is evaluated by comparing the model's results to the CMEMS tide-gauge observations. The average peak differences during extreme events for the non-coupled model (E2) and the fully coupled model (E3) are displayed in Figure 3.7. The blue colours mean that the storm surge peak is underestimated compared to the observations while red colours indicate an overestimation. For both with and without the wave coupling inclusion, the models globally under-estimate the storm surge peaks in average by -13 cm and -11 cm for E2 and E3 respectively. Most of the differences occur on NWS with a maximal change in the error from -61 cm to -52 cm (+9 cm). A few areas show also small localised overpredictions mainly along the English Channel and the Iberian Mediterranean coast and Corsica. To assess the impact of the wave process inclusion, the difference in performance between the non-coupled and fully coupled experiments is directly displayed in Figure 3.8. The blue colour indicates an improvement of the result by including the wave coupling while the red shows a degradation. Globally, the performance is slightly improved by the coupling (error reduced by -0.2cm, 2%). Most of the positive changes are situated in the German Bight. On the contrary the results are slightly worsened along the English Channel and especially on the Northern part of France near Dunkerque, at Peniche (Portugal) and more mildly around the Gulf of Lyon.

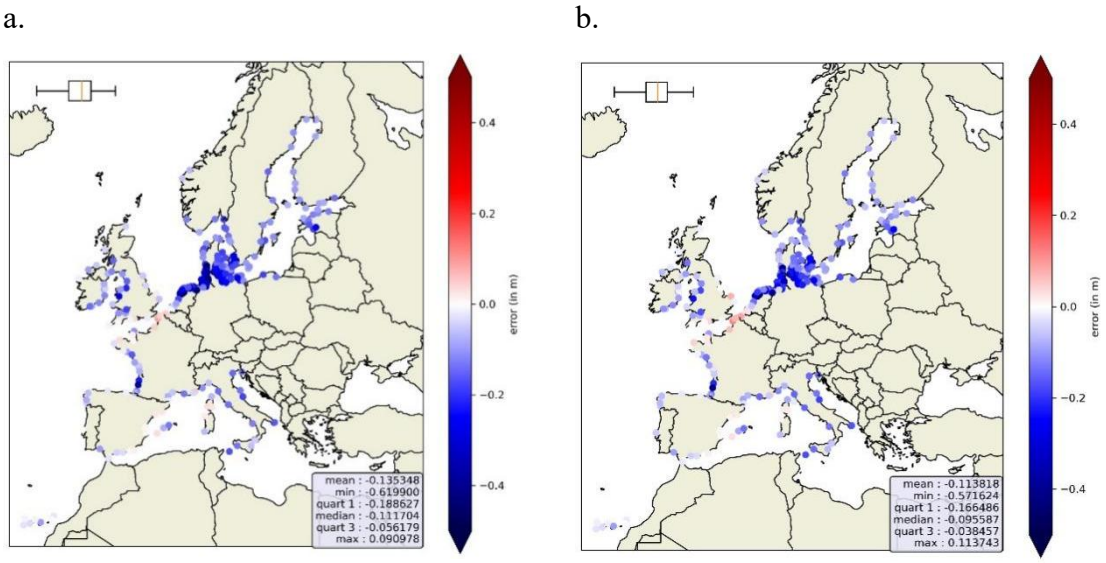

Figure 3.7 Surge peak magnitude error [m] against observed data for a. the uncoupled wave and b. the fully coupled models.

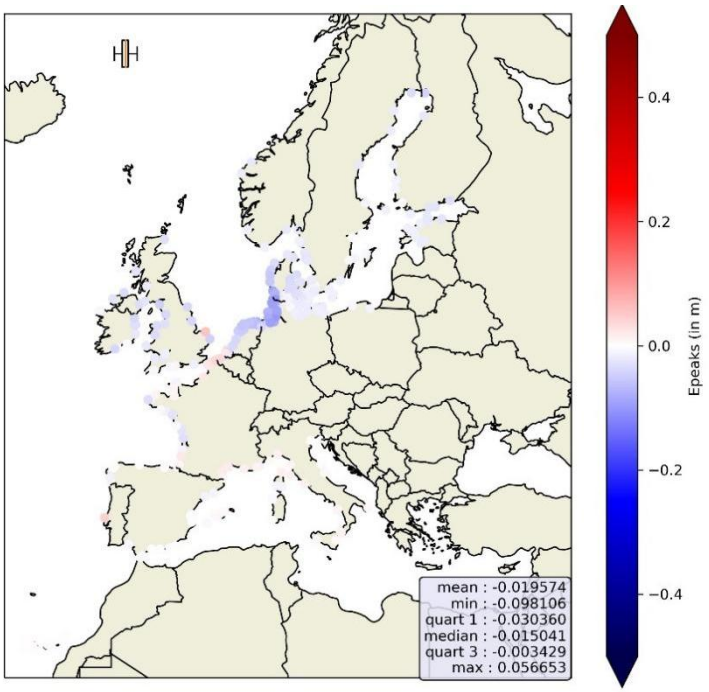

Figure 3.8 Absolute error difference [m] between the uncoupled and fully coupled model.

3.2 CMEMS-IBI model

3.2.1 Wave coupling effects

First, the wave coupling impacts for average conditions are evaluated. The annual centred Root Mean Square (RMS) of the change in the signal is computed as an indicator of changes in

variability, which is normalized by the variability of the non-coupled run (control run). Figure 3.9 shows the spatial distribution of this change when including the Stokes-Coriolis coupling process (panel a) and when including all wave-coupling processes (panel b) for 2018 for the NTR (surge). The impact on the WL has also been evaluated and it is discussed but not shown here.

a. b. c.

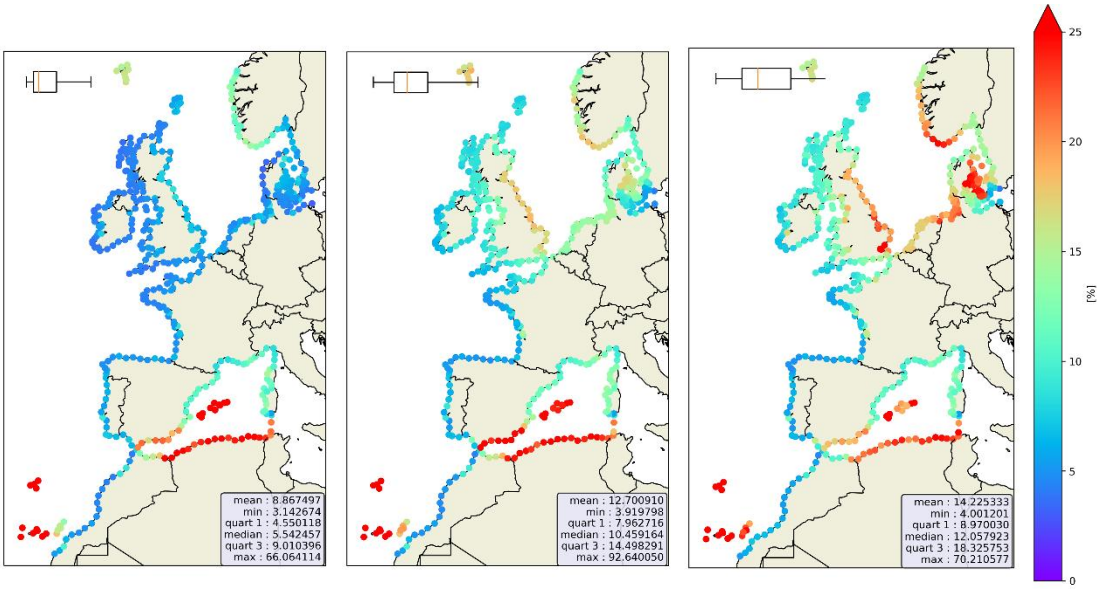

Figure 3.9 Normalized standard deviation [%] of the difference between uncoupled and wave-coupled runs. a.- stokes experiment. b.- tauoc experiment and c.-cb experiment (fully coupled) . See Table 2.1 for explanation of the different experiments.

For WL, the median change showed moderate values for the fully coupled case (2.5%), while it is 12% for the NTR. The change is indeed more evident for the NTR as the impact of wave coupling on tides appears negligible, and therefore the WL normalized change in tidally dominated regions (Atlantic, Northwest Shelf) significantly reduces. For water-levels, significant changes are seen in the western Mediterranean as well as around the Skagerrak/Kattegat and Danish Straits (>20%), while for NTR additionally the Canary Islands, Madeira and the North Sea also stand out. Looking at the evolution of the impacts with increasing level of coupling (from panel a to c in Figure 3.9), it is revealed that changes are dominated by the momentum flux modification across the domain. In average and for the NTR (stronger impacts than WL), the stokes drift has an impact of 5.5%, with the momentum flux notably increasing the impact to 10.4%, and finally the wave induced mixing mildly increasing the impact to 12%. Wave induced mixing impacts are concentrated around the North Sea and

Danish straits, as well as around some estuaries (e.g., Gironde Estuary, FR). In contrast to the overall trend, the western Mediterranean (including the Balearic Islands) and mid-ocean island chains (Canaries, Madeira) show comparable impacts for all three coupling components. In particular for the Balearic Islands, the change in variability concerns both seasonal and non-tidal, high frequency (NTR) signals. A closer look at the extracted tide (which includes the seasonal solar components – solar annual SA, solar semi-annual SSA) for non-coupled and coupled runs at the Ibiza TG shows significant changes in these seasonal components (not shown).

A closer inspection on the coupling impacts reveals that in these regions where comparable impacts for all three components are observed, the impact is indeed affecting the sea level signal throughout the year and can indeed be associated to a general change in variability under average conditions (Figure 3.10-a). For the NWS however, the changes in the sea levels appear highly correlated with peak surge events, therefore suggesting that what appears as a change is annual average conditions is in reality a change during extreme conditions which results in elevated values of the annual RMS of the change (Figure 3.10 -b). Hence, the impacts during extreme events are evaluated in the following section.

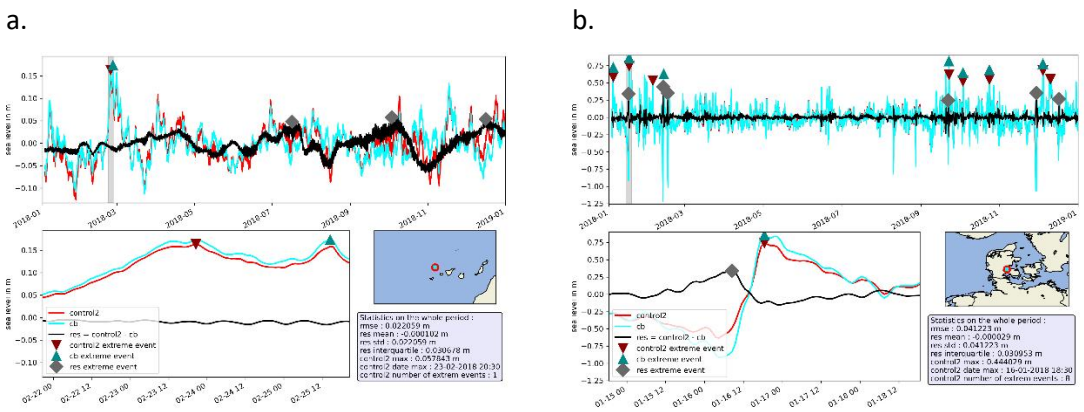

Figure 3.10 NTR signals for non-coupled (red) and fully coupled (blue) simulations, with a zoom on the annual largest event. Triangles point to the peak values above the 99th percentile for each simulation, while diamonds show the maxima of the residual signal (uncoupled - coupled). a: example of coupling inducing changes in annual variability in the Canary Islands. b: Example of coupling inducing changes during extreme NTR events in the Danish Straits.

Figure 3.11 shows the average changes in the WL and NTR peak magnitudes during the detected extreme events, respectively. Note than only the extremes commonly identified by the different experiments are considered. For both components, it is observed that those locations showing an important impact due to wave coupling show generally an increase of the peaks (red colours). Significant impacts are limited to the Southern North Sea and Baltic

entrance regions for WLs, while NTR show a more widespread impact across the NWS. Highest values concentrate in the German Bight, with WLs and NTR increasing up to +40 cm (+23%/32% for WL/NTR). The only exception is the Balearic Islands where a decrease is obtained. Here, compensating effects of the 3 coupling components are observed, with stokes drift decreasing the peaks, the momentum modification increasing them, and finally the mixing reducing them again. This effect is also more visible for WLs than for NTR, indicating that the main change responsible is the shift in the annual/semi-annual signals described previously. In terms of relative importance of the difference coupling components, the Stokes drift shows generally negligible impacts (median 0.3% for WLs, 2.3% for NTR) other than in the NWS for the NTR component (+5%, maximum absolute values of 7 cm in the German Bight). The momentum modification shows again to be the main driver of the significant impacts seen in Figure 3.11. The impact of the wave induced mixing is concentrated around the Southern North Sea, Danish Straits and Eastern Irish Sea, where peaks further increase. The regions that are negligibly impacted in terms of both peak NTRs and WLs are the Iberian Peninsula (with some exceptions such as Cadiz) and the Côte d'Azur.

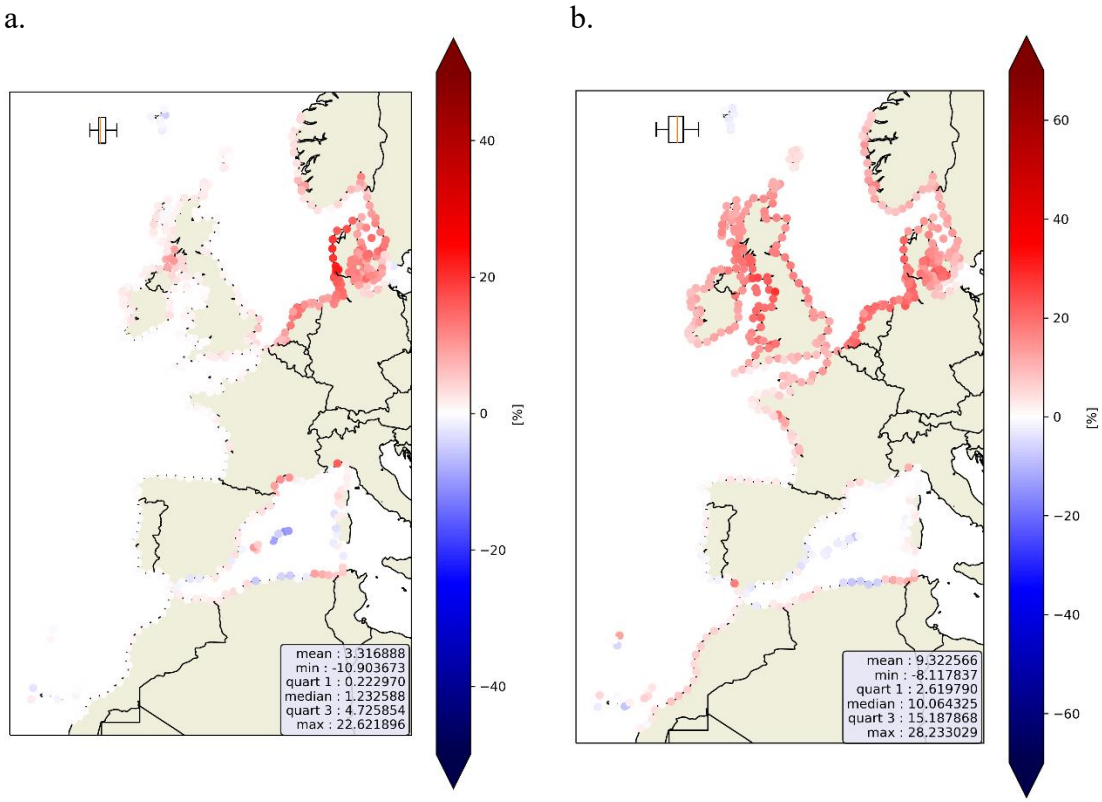

Figure 3.11 Normalized [%] impact of the wave-coupling on the average extreme WLs (a) and surges (b) over the detected extreme events. Note the colour bar limits are different between the panels.

Figure 3.12 shows the NTR time-series for a location around Hoek van Holland (Dutch coast), with a zoomed view during the storm Eleanor in early January 2018. While this storm generated the annual largest water-level, it is clear from Figure 3.12 that there was another storm later that month (storm David/Friederike) inducing even higher surges, for which the wave coupling induces an even stronger increase (close to +50cm, +50%). Figure 3.13 shows the effects of wave coupling during the storm Emma in early March 2018 at Sète, French Mediterranean coast. In this case, a significant (+10cm) impact is seen on the surge due to the momentum modification, interestingly hours before the actual surge maxima for which the increase is more limited. This earlier increase in the surge actually coincides with the event maximum WL time which increases accordingly (+9cm), highlighting the important of the coupling for flood risk.

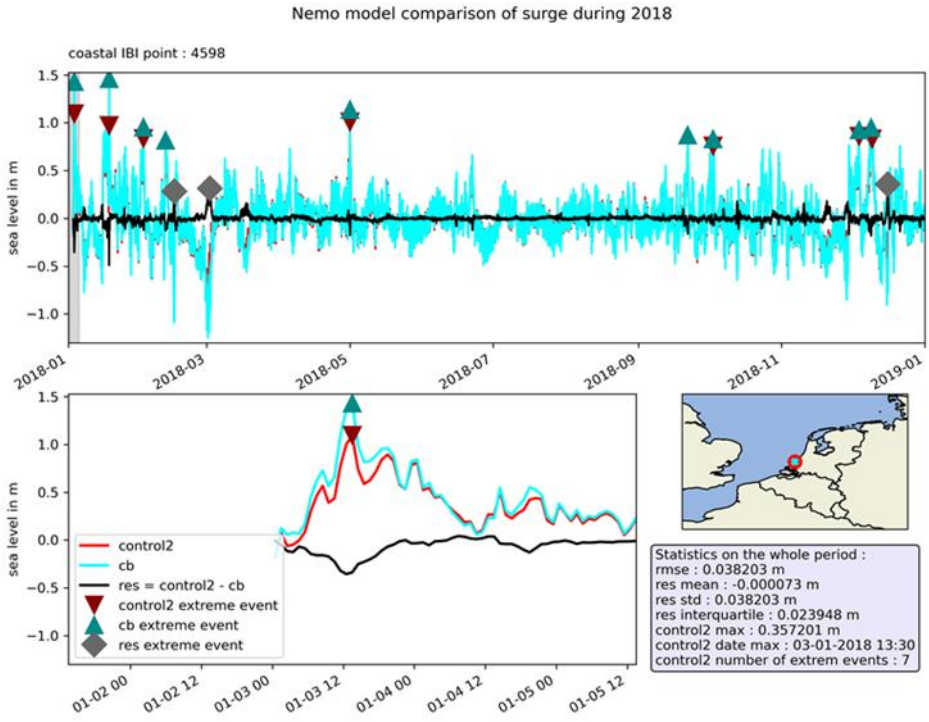

Figure 3.12 Modelled surge series for uncoupled (red) and coupled (blue) simulations, with difference in black, for the Hoek van Holland TG location. Triangles depict the peak values during the corresponding extreme events. Top: full year (2018). Bottom: Eleanor storm in January 2018.

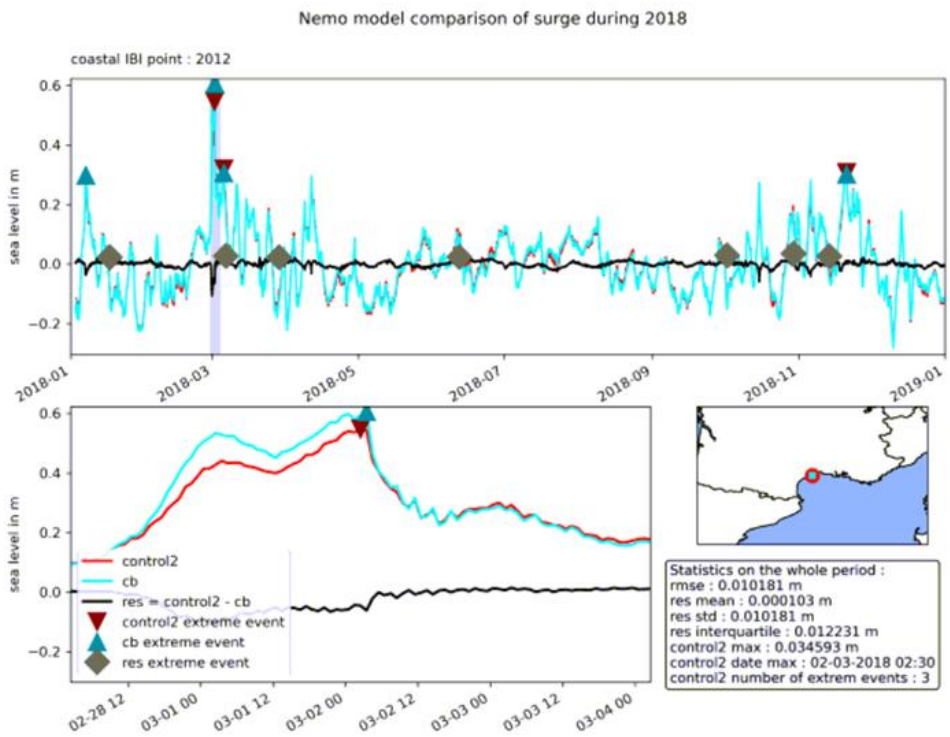

Figure 3.13 Modelled surge series for uncoupled (red) and coupled (blue) simulations, with difference in black, for the Sète TG location. Triangles depict the peak values during the corresponding extreme events. Top: full year (2018). Bottom: Emma storm in March 2018.

3.2.2 Impact on model performance

In this section, we will evaluate the impact of the wave coupling in terms of model performance for coastal water-levels, using the CMEMS tide-gauges as observations. Given that results in the previous sections show that the main relative impact of wave coupling is on the extreme events and given the main focus of ECFAS of performance for marine storms, the following results focus on the skill metrics during detected extreme events.

Figure 3.14 and Figure 3.15 show the change in the peak magnitude error, averaged across the storms detected per tide-gauge, for extreme WLs and NTRs respectively. Note that the extreme WLs have been identified using a combination of thresholds for WLs and NTR (99.9th and 99th, following **D4.1 – Report on the calibration and validation of hindcasts and forecasts of TWL** in order to focus on storm-induced extremes and avoid purely tidal extremes. As for the NTR, the extremes have been selected using uniquely a threshold for the NTR (since it is already correlated to storminess), using a 99th percentile, and are therefore independent of the WL extreme events. In this way, one can appreciate the wave coupling on storms that randomly happened in lower tide conditions but that in principle, could have led to extreme

WLs/flooding under a different tidal phase. These methods lead to an average number of storms per TG of 2 for the WLs and 9 for NTR. Median peak WL error (Figure 3.14) reduces from -18 cm to -10 cm (-10% to -5%, not shown), with an even larger median magnitude reduction for the NTR (Figure 3.15 Peak NTR error (model – observed) across detected storms for uncoupled (left) and wave-coupled (right) simulations. NTR-only determined extremes (99pct)., from -19 cm to -7cm, -24% to -11.5% in normalized terms -not shown). Given the significant surge contribution in the detected WL extremes, the spatial patterns for both components are similar. The reduction is most pronounced in the NWS. The consistent improvement of the model across the domain is remarkable, stemming from the consistently underpredicted extremes in the non-coupled simulation and from the consistently increased extremes induced by the coupling. The positive impact is also seen locally in other regions further south such as the coast of Cadiz, Gulf of Lyon and Atlantic French coast/northern Spain.

a. b.

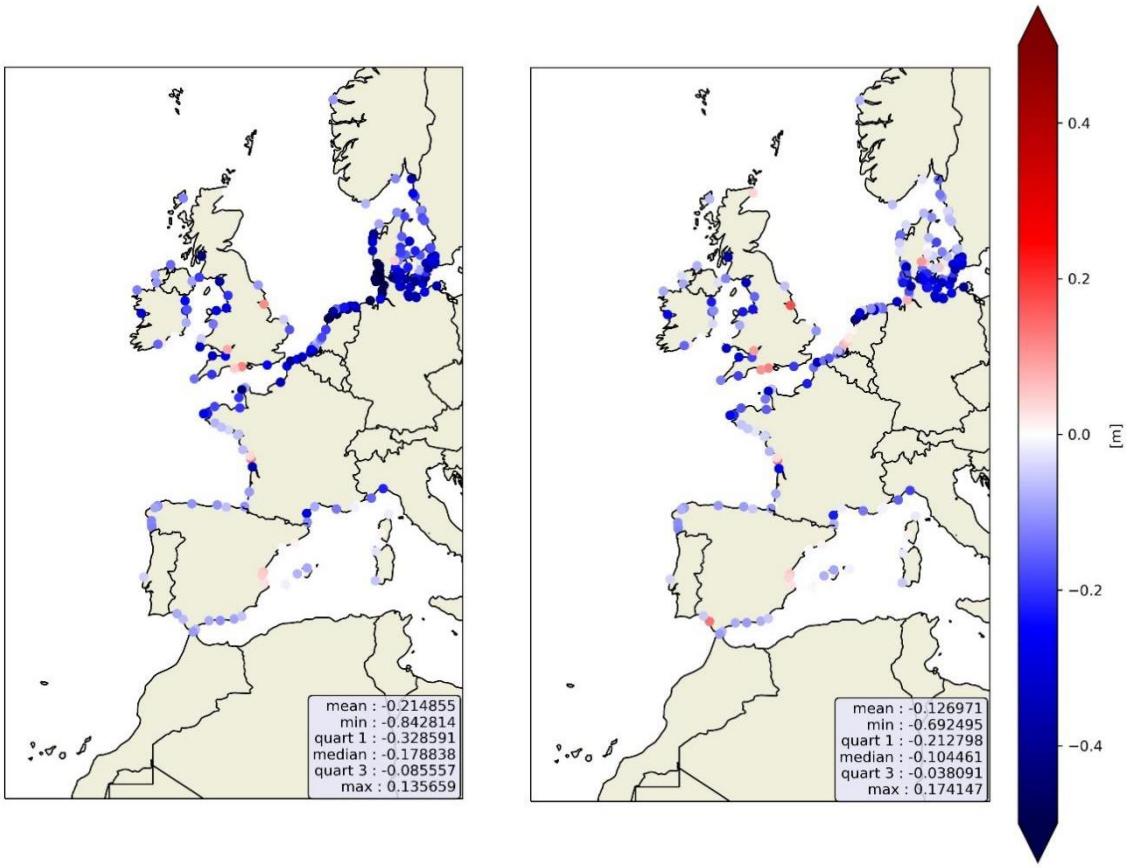

Figure 3.14 Peak WL error (model – observed) across detected storms for uncoupled (a) and wave-coupled (b) simulations. Extremes determined by concurrent WL and NTR extremes (99.9th and 99th percentiles, respectively).

a.

b.

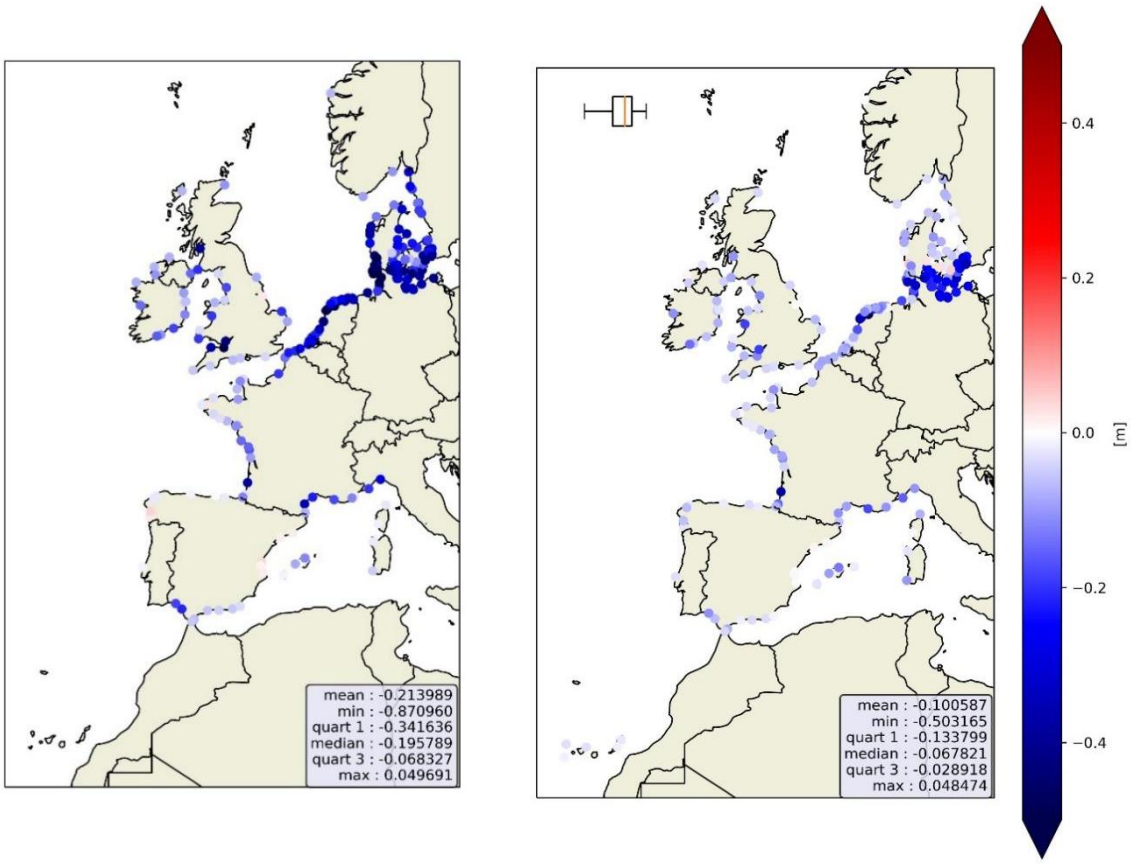

Figure 3.15 Peak NTR error (model – observed) across detected storms for uncoupled (left) and wave-coupled (right) simulations. NTR-only determined extremes (99pct).

4 Model inter-comparison

In this section, the relative impact of the wave coupling in the coastal TWLs (section 3) are compared between the CMEMS and ANYEU-SSL systems. Such comparison will support the discussion on what modelling components are cost-effective for each type of modelling system and why. Additionally, the skill of the models for the representation of coastal water-levels is compared at a qualitative level. The skill comparison is kept at a qualitative level because of the numerous model configuration differences that make a quantitative, direct comparison illegitimate. These differences are summarized in Table 4.1. In particular, the different forcing products employed - which target different type of WL reconstructions (reanalysis, operational) – make a direct comparison extremely challenging, due to the strong focus of the assessment on marine storms.

Table 4.1 Description of the main differences between ANYEU-SSL and CMEMS-IBI models used for intercomparison that may lead to differences in the WL representation and its sensitivity to certain physical processes.

Model	Atm.forcing	Resolution	Bathymetry capping	Wave Ocean coupling	Ocean Wave coupling
ANYEU-SSL	ERA5 (~30km)	2.5km (coast)-25km (deep water)	10 meters	• Wave radiation stress • Wind. Stress	• Surface Currents (2DH) • WL
CMEMS	ECMWF-IFS (10-15km)	~2-3km uniform	5 meters	• Stokes • Wind. Stress • Wave induced mixing	• Surface Currents (3D)

Besides differences in the baseline model skill, substantial model differences in the geometrical definition of the coastal zone may also impact the sensitivity of the models in such regions to processes such as wave coupling. Figure 4.1 illustrates the differences in the coastal representation between ANYEU-SSL and CMEMS-IBI stemming from their geometrical differences (bathymetry, coastline, and resolution) along the complex region of the Southern North Sea. It is evident that in this region the bathymetry capping leads to a strong difference between the models, as well the land mask used and coastline definition, as this area is characterized by a complex coastline with multiple estuaries and small islands. Furthermore, small-scaled bathymetric features are present in both shallow and further offshore areas, which show smoother patterns in the ANYEU-SSL model than in the CMEMS-IBI model, resulting from the lower spatial resolution of the former away from the coast. While the

Southern North Sea is the region showing strongest differences in coastal representation, other coastal stretches across the Northwest Shelf also show important differences due to the bathymetry capping, effectively making ANYEU-SSL consistently deeper at the coast. Further south, the continental shelf narrows, leading to smaller differences in the coastal bathymetry at the given resolutions.

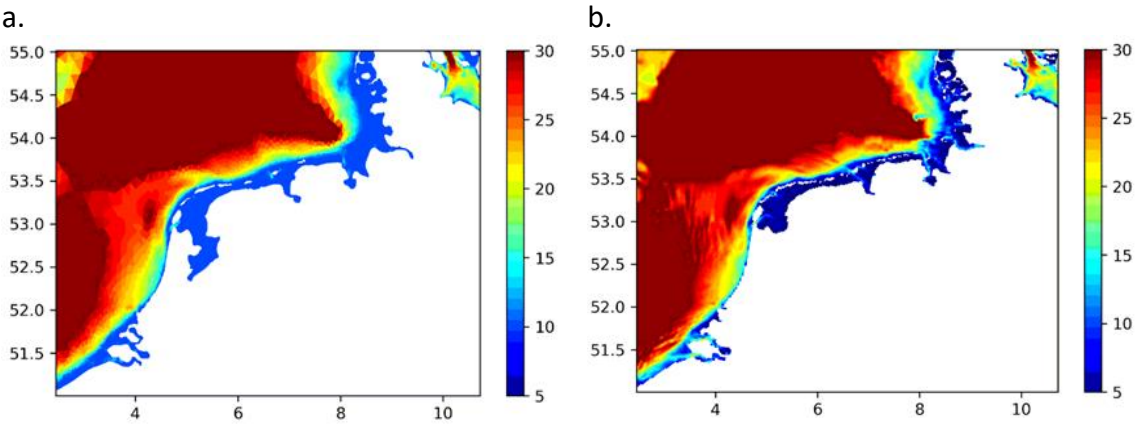

Figure 4.1 Model bathymetry [m] in the Southern North Sea region for the ANYEU-SSL model (a) and CMEMS IBI model (b).

4.1 Wave coupling effects

First, the relative impact of wave coupling on average conditions is compared. Note that the normalized metrics for annual statistics are normalized by the baseline variability in the model, which can be different between a 2D and a 3D model. Especially for micro-tidal environments and strongly baroclinic environments such as the Mediterranean Sea.

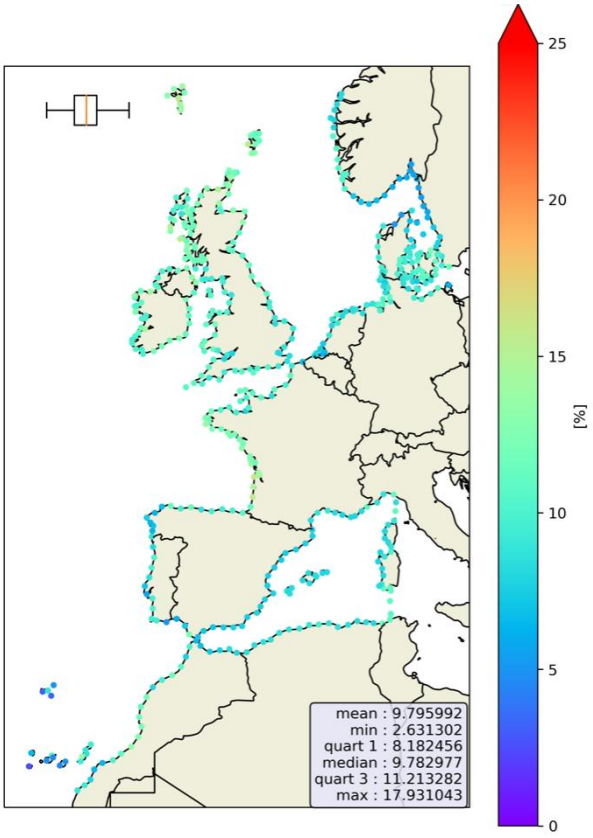

Figure 4.2 Normalized standard deviation [%] of the difference between uncoupled and wave-coupled runs for the ANYEU-SSL model, plotted at the identified common coastal points with the CMEMS-IBI model.

Figure 4.2 shows the normalized standard deviation of the relative impact of the wave-coupling in ANYEU-SSL over 2018 at the identified common coastal points between the CMEMS-IBI and ANYEU-SSL models. When comparing Figure 4.2 to the corresponding figure for CMEMS-IBI (Figure 3.9-c) it is evident that, while the median relative impact is comparable for both systems (9.7% and 12% for ANYEU-SSL and CMEMS-IBI respectively) the CMEMS-IBI model shows much stronger regional differences than ANYEU-SSL. In terms of magnitudes, CMEMS-IBI shows a stronger (and highest) impact of the coupling in the North Sea, while ANYEU-SSL shows stronger impact than CMEMS-IBI along the Atlantic façade of the domain and the Bay of Biscay. A time-series along the French Atlantic façade showing enhanced wave coupling effects for ANYEU-SSL (Figure 4.3-c, French Basque coast) reveals that wave coupling impact is not in fact uniform across the year but stronger in winter, and not necessarily correlated with high surge events (extremes). This effect is not observed in the CMEMS-IBI model (Figure 4.3-d). On the contrary, the strong variability impact around island chains described in section c.3.2 for CMEM-IBI (Figure 4.3-b) is not found in the ANYEU-SSL model (Figure 4.3-a). This points to a baroclinic nature of the wave coupling impacts in these regions.

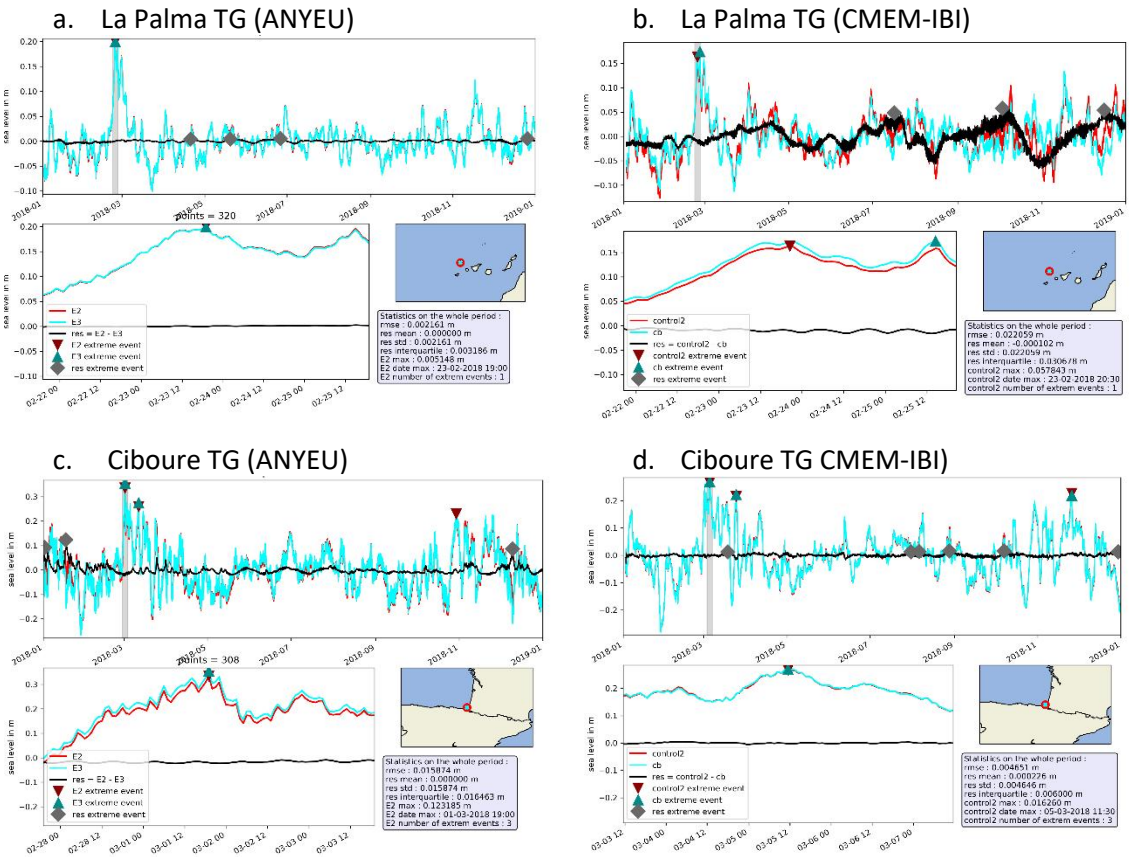

Figure 4.3 Time-series of modelled NTR for multiple TG locations for non-coupled (red) and coupled(blue) simulations. The black line indicated the difference between the two. a. and c. are results from the ANYEU-SSL model, while b. and c. are from the CMEMS-IBI simulations.

Next, the trends of the impact of wave coupling during extremes are compared. As elaborated in section 3.2.1., CMEMS-IBI shows significantly and consistently increased peak values during extreme events induced by wave-coupling concentrated around the Northwest Shelf region (>25% increase; Figure 3.11), with much smaller relative impacts further south in the rest of the domain. The ANYEU-SSL model, instead, shows a factor 2 to 3 smaller amplitude of the impacts in general (~10%; Figure 3.5). Indeed, the times-series plot in Figure 4.4 for Hoek van Holland with a closeup on the storm Eleanor shows a negligible effect of the coupling for the ANYEU-SSL model extreme surges (Figure 4.4-a), while the impact for the CMEMS-IBI model was in order of 35-40 cm for Eleanor and similar magnitude events (Figure 4.4-b). Furthermore, the models show a somewhat different spatial pattern of the wave coupling impacts on extremes. While both models agree on increased extreme NTR values in the NWS region, the ANYEU-SSL model shows a substantial decrease of the extreme values (-10%) across the Portuguese and Moroccan Atlantic coasts (Figure 3.5), while CMEMS-IBI model shows either unchanged or somewhat increased extremes (Figure 3.11). A closer look at one of these

coastal time-series along the Portuguese coast (Peniche TG, Figure 4.5) confirms that indeed, the impact (black line) appears correlated with the surge magnitude, with largest impacts during the storm Emma in early March 2018 (decrease of ~8 cm). This timeseries also reveals that the impact of coupling outside the extreme event follows previous observations in similar kind of environments (Figure 4.3-c - narrow shelf, ocean swell exposed location) where a higher variability of the impact was seen throughout the winter season. For the CMEMS-IBI model, no evident impact is seen at this location for either extreme or average/winter conditions (not shown). The trend of decreasing extremes is also seen across the Mediterranean for ANYEU-SSL, strongest on the central and eastern side of the basin, which is unfortunately out of the domain coverage of CMEMS-IBI and therefore not comparable. Nonetheless, in the western Mediterranean, both models show generally negligible wave coupling impacts along the coast other than in Balearic Islands, with both models showing a decrease in extremes (in the CMEMS-IBI model being a consequence of a change in average conditions, see section 3.2.1), and the Gulf of Lyon, where ANYEU-SSL shows a mild decrease while CMEMS-IBI shows no impacts.

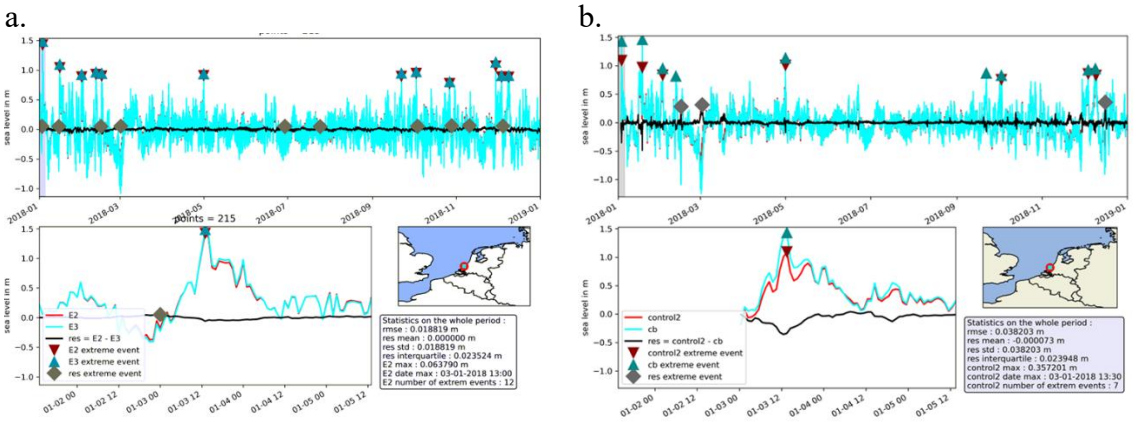

Figure 4.4 Modelled surge series for uncoupled (red) and coupled (blue) simulations, with difference in black, for the Hoek van Holland TG location. Triangles depict the peak values during the corresponding extreme events. Top: full year (2018). Bottom: Eleanor storm in January 2018. a. ANYEU-SSL model. b. CMEMS-IBI model.

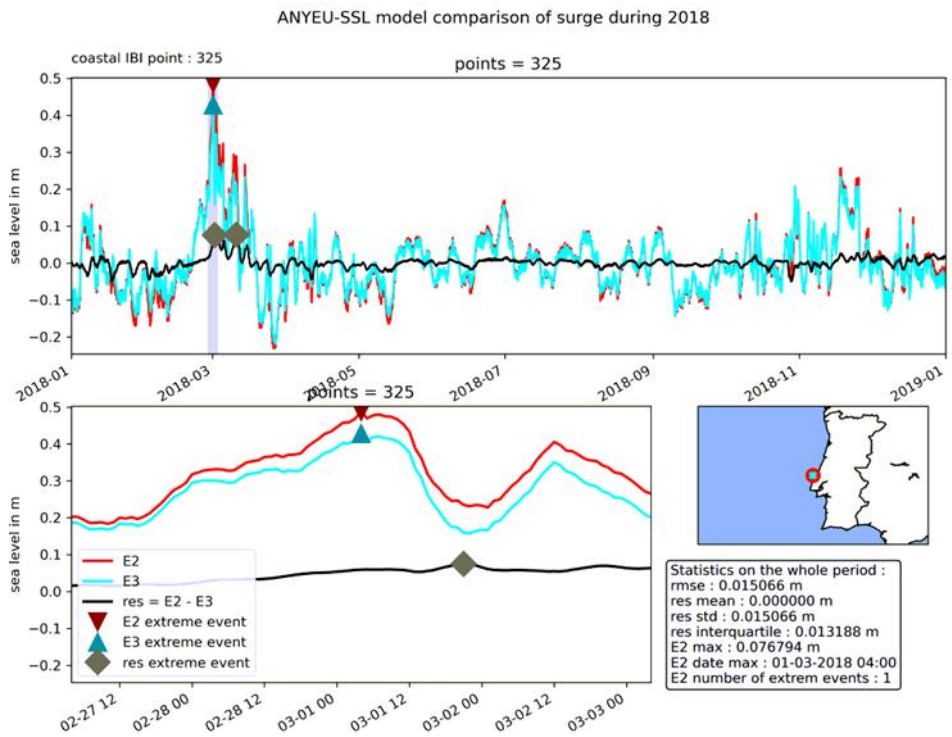

Figure 4.5 ANYEU-SSL modelled surge series for uncoupled (red) and coupled (blue) simulations, with difference in black, for the Peniche TG location. Triangles depict the peak values during the corresponding extreme events. Top: full year (2018). Bottom: Emma storm in March 2018.

A summary of the impact of the evaluated settings on yearly average and extreme conditions, in terms or relative model changes as well as changes in performance against tide-gauges, is shown in Table 4.2 and Table 4.3 for the ANYEU-SSL and CMEMS-IBI models respectively.

Table 4.2 Summary of normalized metrics derived for the different model experiments for ANYEU-SSL on the yearly average and extreme statistics. The first column indicates the simulations compared. The control denotes the simulation without any of the evaluated processes included (tide-surge, wave-surge interactions). TG indicates the comparison against tide-gauge records. WCM: wave coupled model, TCM: tidally-coupled model. Median, first quantile and third quantile across all evaluated points is shown (coastal points for intra-model comparisons, tide-gauge locations for the comparison against TG. N.A: not evaluated.

ANYEU-SSL	Yearly influence – RMSE_NG (%)			Extreme-events – normalized peak difference (%)		
	Median	1rst Quantile	3rd Quantile	Median	1rst Quantile	3rd Quantile
TCM - control	14.67	10.72	21.56	-1.14	-2.83	0.54
WCM - control	9.37	.7.80	11.31	0	-4.22	3.32
control - TG	. N.A	N.A.	. N.A	-19.02	-27.02	-10.34
WCM - TG	N.A.	N.A.	N.A.	-16.04	-24.66	-6.43

Table 4.3 Summary of normalized metrics derived for the different model experiments for CMEMS-IBI on the yearly average and extreme statistics. The first column indicates the simulations compared. The control denotes the simulation without any of the evaluated processes included (wave-surge interactions). See Table 4.2 for further explanation.

CMEMS-IBI	Yearly influence – RMSE_NG (%)			Extreme-events – normalized peak difference (%)		
	Median	1st Quantile	3rd Quantile	Median	1st Quantile	3rd Quantile
WCM -control	12.05	8.97	18.32	10.06	2.6	15.18
Control - TG	. N.A	N.A.	N.A.	-20.92	-28.49	-14.54
WCM - TG	. N.A	N.A.	N.A.	-10.50	-21.69	-6.15

5 Discussion

In this assessment, the importance of the interaction between a number of physical processes in the modulation of coastal water-levels and their extremes is evaluated by performing sensitivity simulations with state-of-the-art ocean and wave modelling systems. Several studies exist in the literature that targeted similar questions for similar regions and conditions, which are here used for benchmarking and to support the findings of this study.

As stressed by a few reviewing works (Idier et al., 2019; Wolf, 2009; Woodworth et al., 2019), coastal water level can be decomposed into numerous components. Each of these components interact creating a complex physical process scheme as illustrated by Idier et al. (2019) , see Figure 5.1. In their work, the authors reviewed the possible interactions and mechanisms. However, in the present work only two types of interaction are considered: the wave and atmospheric surge interaction and the tide and atmospheric surge interaction.

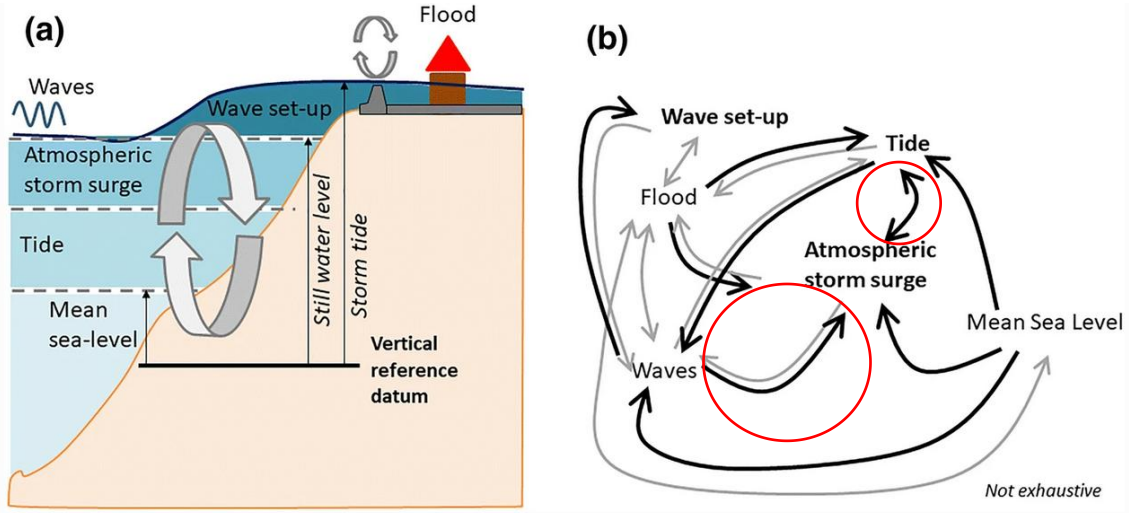

a Components of storm tide, terminology and sketch of interactions. **b** Main interactions between mean sea level, waves, atmospheric storm surges, tide, wave setup and flooding. In bold and black: the focus of the present paper

Figure 5.1 Graph of water level components and their non-linear interactions, extracted from the work of Idier et al. 2019. In red circles in panel b, the interaction processes studied in the present work.

The interaction between tide and surge has deeply been studied in the past. The non-linear tide and surge interactions were recognised important in shallow water areas with large tidal range (Wolf, 2009). In the present work, only the ANYEU-SSL model was used to evaluate this interaction. A strong influence is detected on the NWS matching this theory (Figure 3.1 and Figure 3.2). Changes on the peak surge larger than 20 cm are detected on the German Bight and in the order of 12 cm along the Eastern coast of the UK matching the findings of Horsburgh & Wilson (2007). The English Channel seems also to be moderately affected by this interaction

(order of 12 cm) on its eastern section and decreasing westwards towards Brittany, behaviours also reported by Idier et al. (2012) and Arns et al. (2015). The improvement of the surge prediction by the dynamic coupling with tide models was also previously assessed by Fernández-Montblanc et al. (2019) on the previous version of ANYEU-SSL, with a slightly coarser resolution at the coast and the ERA-Interim atmospheric model forcing. In this previous work, a clear improvement of the predictive skill was identified in comparison to tidal gauges available from the JRC Sea Level Database (http://webcritech.jrc.ec.europa.eu/SeaLevelsDb) and EMODNET web site (http://www.emodnet-physics.eu/Map/). Due to the strong similarity of the present ANYEU-SSL model and that of Fernandez-Montblanc et al. (2019), the inclusion of the tidal coupling is expected to improve the predictive skill in this new version of the model.

Concerning the wave and atmospheric surge interaction, as one of the most comparable, recent and relevant studies, Staneva et al. (2017) performed a similar modelling study based on the NEMO code (as is used for the CMEMS-IBI model), focusing on the Northwest Shelf region, where the importance of the different coupling components was also evaluated (Stokes-Coriolis, momentum flux and turbulent kinetic energy flux modification by wave coupling). For 2 historical storms hitting the North Sea, they reported a wave coupling induced increase in extreme surges of several decimetres along the Southern North Sea, with maximum increase of ~40 cm (>30%) around the German Bight, remarkably agreeing with the results shown in this report for the CMEMS-IBI model (Figure 3.11) despite the different periods/storm events considered. They show that the enhancement of surge maxima is not limited to the coast but extends far offshore, where it can still reach 10-20 cm. Also, in line with the findings in this report, Staneva et al. (2017) conclude that the impact is mostly attributed to the momentum flux modification. However, they find a stronger relative contribution of the Stokes-Coriolis component than the one reported in this document, which is potentially related to the differences in wind patterns and wave propagation between the different storm events. In terms of the turbulent kinetic energy flux modification, they focus on different aspects of this component and therefore results are not directly comparable. In another modelling study which focused on the German Bight area, Staneva et al. (2016) found similar if not stronger wave-induced impacts (up to +70 cm /+40%) on extreme surges in the region, resulting in a much better agreement against local tide-gauges. In a comparable study, also using the NEMO code and WAM for wave coupling and looking at a longer period of 9 years, Bonaduce et al. (2020) found significant wave-induced impacts on surges at varying time

and spatial scales, with a 30-40% reduction of the surge RMSE for low frequencies (30-90 days), similar impacts for frequencies between 1-5 days and lower impacts (<10%) below 12 hours. The lower frequency contribution point to wave-induced changes in the circulation and can be associated with the low-frequency change in variability observed in the surge signal for the CMEMS-IBI model in ocean-exposed coasts around island chains. Also, in line with the results seen for island-chains in the CMEMS-IBI model experiments, Bonaduce et al. (2020) show a significant contribution of all wave-coupling components in deeper waters, stemming from changes to the mesoscale dynamics, while wave-surge interaction on the shelf appears clearly dominated by the momentum flux modification. When looking at extremes (99.9th percentile), they find an increase in the order of 60-80 cm in autumn/winter seasons, as well as a significant increase of summer extremes (+30 cm). Given these benchmarking studies, it is concluded that all the studies involving 3D ocean models and comparable wave-coupling processes notably agree on the magnitudes and spatial distribution of the wave non-linear contributions to surges and their extremes. A remarkable feature, highlighted by all aforementioned studies and the results in this report, is that over the continental shelf, the wave-induced change in momentum flux is dominating the wave coupling interactions. In the momentum flux modification, it is the change in wind drag that is responsible for most of the change (Stéphane Law Chune, Mercator Ocean, personal communication). As such, wave-coupling impacts on coastal surges appear strongest during stormy, strong wind conditions. The strong coastal sensitivity to the momentum flux change is associated to the increased effectiveness of the wind stress in continental shallow waters. Therefore, being the wind stress an external, surface (2D) force to the ocean model, 2DH models should be well suited to represent this dominant wave-coupling effect on the continental shelf.

With this principle in mind, the 2DH ANYEU-SSL model trends for wave-induced effects are benchmarked against other depth-averaged modelling studies in literature. In the validation exercise of the SELFE-WWM II coupling, Roland et al. (2012) developed models of the hurricane Isabel (2003) hitting the North Carolina coast in the US, considering both 2D and 3D version of the circulation model and with and without WWM II wave coupling. Note that the hydrodynamic model SELFE is the predecessor code of SCHISM, and therefore largely resembles the code behind ANYEU-SSL. For both configurations, adding the wave coupling improves the predictive skills by 2%, similarly than reported here. However, Bertin et al. (2015), using the SELFE- WWII code system in its 2DH form like ANYEU, obtained an increase in surge peaks due to wave-dependent wind stress of comparable magnitude to the previously

mentioned 3D studies (+20-35%) for the Xynthia storm (2010) in the Bay of Biscay, bringing again the originally under-predicted surges closer to observations. They argue that the increase in wind stress (by a factor 2) and hence peak surge was due to the young sea state conditions during the storm of interest (short, high frequency waves resulting from limited-fetch wave growth) while only an increase of 2-15% is estimated for the Joachim storm (2011) characterized by a different sea state (large and long period waves). The dependency between wave-enhanced surface roughness and wave age was confirmed by Pineau-Guillou et al. (2020) in a depth-averaged modelling study for the North Sea. Compared to these studies, the ANYEU-SSL system shows weaker impacts of the wave-coupling during extremes in the North West Shelf region. The reason behind this is unclear and could be multiple. The bathymetry capping applied at 10 meters could be partly responsible for this underestimation, noting that the corresponding wave-model is also subject to such bathymetry capping. In Bertin et al. (2015) , the numerical grid has a resolution varying between 30 km offshore to 25m at the coast which is 100 times finer than the current ANYEU-SSL resolution at the coast. This difference in the geometry could also contribute to a higher sensitivity of WLs to wave-coupling for this model. Additionally, the momentum flux absorption by the growing waves and released by breaking waves is not taken into account in the ANYEU-SSL configuration, although this effect is considered to be of second order compared to the modified surface drag (Stéphane Law Chune, Mercator Ocean, personal communication). Potentially underpredicted winds within ERA5 compared to ECMWF-IFS could also partly respond to this difference in trend, although Bonaduce et al. (2020) found impacts of expected amplitudes using the ERA5 forcing product. Another potentially important difference between the two models is that the ANYEU-SSL model includes on-line coupling, where the wave information reinjected into the ocean model is derived from a wave field that has already seen the ocean (currents, water-levels), while in the CMEMS-IBI model experiments the ocean model uses wave information that hasn't seen the ocean first.

It is important to understand that, beyond the physical processes in place, the choice of parameterization for the computation of the wind stress will also influence the trends observed when changing to a wave-dependent parameterization. Wind-stress parameterizations (without wave effects) are wide and varied, and often involve user defined coefficients to somewhat calibrate them to the conditions of interest. Typically, the wind stress computation results from establishing relationships between the wind speed at 10 meters and the drag coefficient (most direct way, e.g., Smith & Banke, 1975), or more indirectly through a

relationship with the roughness length, which includes the Charnock relationship (CMEMS-IBI) or the Pond & Pickard. (1983) formulation (ANYEU-SSL). Furthermore, within the Charnock relationship (generally used in wave models as well as in 2DH hydrodynamic models), parameterizations with a constant, wind -dependent or wave-dependent values exist. Typical Charnock values for wave spectral models range between 0.011 and 0.032, with 0.0185 considered the standard and used, for example, in the ECMWF wind stress calculation when no wave-coupling is included. This is also the case in the CMEMS ocean and wave configurations (Law Chune & Aouf, 2018). For ANYEU-SSL, instead, the wind stress surface is estimated with a sea roughness calculated according to the Pond & Pickard (1983) formulation, where sea roughness increases linearly for low to moderate winds (Bertin et al., 2015). As such, differences in the default (non-wave coupled) computation of the surface roughness (which is used for the control simulations in this study for each modelling system) will strongly determine whether wave-induced surface roughness eventually improves or deteriorates the modelled surges. The little sensitivity to the wave coupling observed in the northern European region of the ANYEU-SSL could be resulting from an over-fitting of the baseline drag coefficient towards (extreme) surges in this region, in such a way that the baseline drag value may be relatively close to that resulting under wave-coupled and extreme conditions. This could also explain the stronger sensitivity observed in the southern European part of the domain where the baseline value is presumably too large. This hypothesis could not be verified given the limited model experiments. Figure 5.2 shows the year-average Charnock values from ERA5 for 2018, clearly showing lower Charnock (roughness) values for the Mediterranean and Black Seas than for the NWS and Baltic regions. When switching to a wave-dependent drag, Charnock values that are closer to the values in Figure 5.2 are expected, as opposed to having a space and time uniform value. In agreement with these annual average values across Europe, modelling studies focusing on the North West Shelf generally use Charnock values in the order of 0.025 (Zijl et al., 2013) while values in the order of 0.01 are used for the Mediterranean (Clementi et al., 2017) . The default uniform value used the CMEMS-IBI model (0.018) is somewhere between the two, well justified as the domain extends between the two regions. In terms of temporal variability, a strong inter-seasonal variability is shown in panels b and c of Figure 5.2. Remarkably the Charnock coefficient during the Eleanor storm (Figure 5.2-d) increases by a factor 2 in the southern North Sea compared to (annual) average conditions, highlighting the strong effect of the sea-state dependent roughness during storms. In the study by Clementi et al. (2017) , which focuses in fact on the wave coupling effects in the CMEMS-

Mediterranean model, they found no significant impacts on ocean fields induced by the wave-induced roughness feedback, although they didn't look at water-levels and their extremes. They do however report an important effect of considering the stability of the boundary layer in the wave model, which by default assumes neutral conditions, but when coupled to the ocean model results in increased (turbulent) drag and consequently in increased extreme wave heights, improving the match with observations. It is noteworthy that this component is not used for coupling in the CMEMS-IBI model experiments in this report, but stability in the boundary later is actually taken into account in the computation of the wind stress in the ocean model. This represents another fundamental difference in the wind stress computation between typical 3D ocean models and 2DH ocean or wave models.

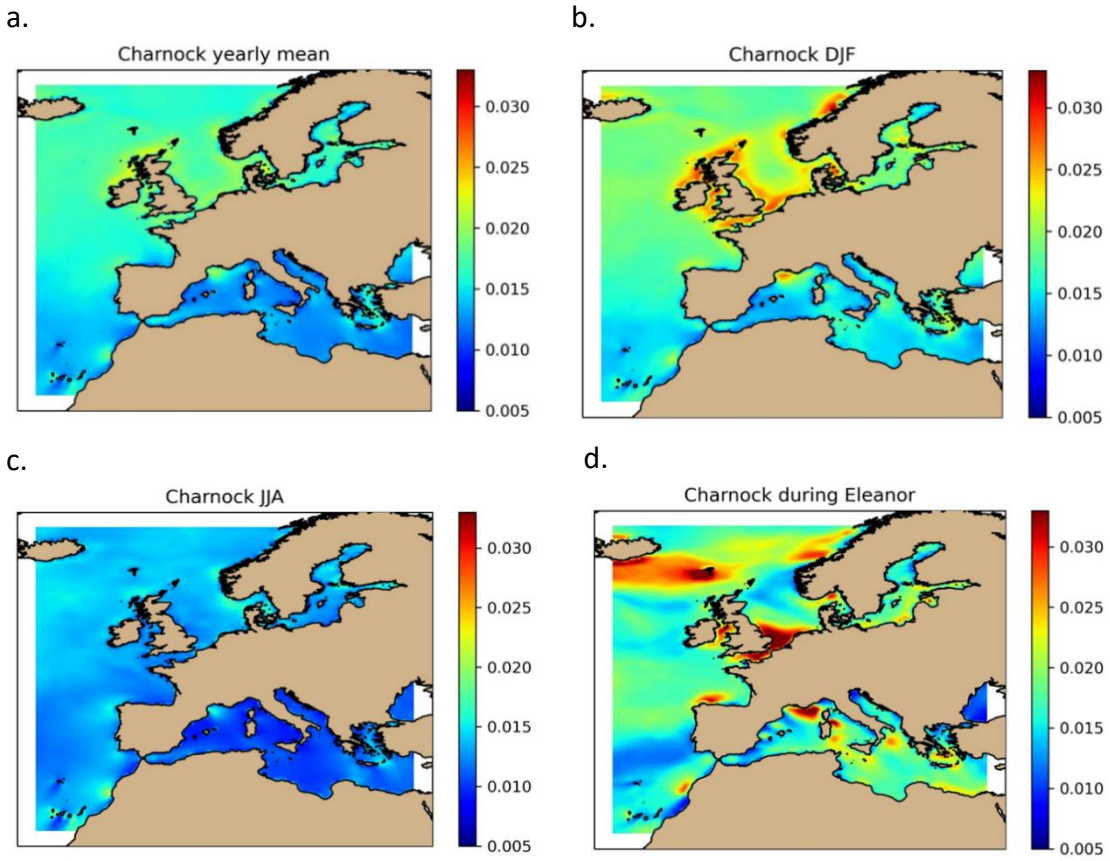

Figure 5.2 Charnock coefficient calculated by the ERA5 reanalysis dataset resulting from coupling to waves. Data retrieved from the Copernicus Climate Data Store (C3S) a. 2018 mean value. b. Winter average. c. Summer average. d. Average during storm Eleanor.

To add to the complexity of the problem, the atmospheric models also use their own parameterization for the sea-roughness. The ECMWF products, for example, use a constant 0.018 Charnock value by default and sea-state dependent values when coupled to their own wave model. The parameterization choice (Charnock in this case) as well as the roughness

coefficient values (uniform/wave dependent) will impact the resulting (10-meter) winds, which is the input information used to force the ocean and wave models. As shown by Pineau-Guillou et al. (2018), wave-dependent surface drag values for the ECMWF operational system may be over-estimated for high winds, leading to underestimated 10-meter winds compared to in-situ observations. Importantly, the 10-meter wind needs translating to wind stress before used for forcing the ocean and wave models. Using the (underestimated) 10-meter winds in combination with the (overestimated) drag coefficient would lead to a consistent wind stress computation. Instead, using the 10-meters winds only together with default (average) roughness values (e.g., Charnock of 0.018) would in principle result in underpredicted wind stresses. This is the approach followed for CMEMS models as well as ANYEU-SSL and could therefore partly explain the systematically underpredicted extreme surges and waves seen for the models in the present work as well as thoroughly reported in **D4.1 – Report on the calibration and validation of hindcasts and forecasts of TWL.**

These inconsistencies between atmosphere, wave and ocean wind-stress calculations lead to increased uncertainties in the computation of storm surges, which are generated at the interface and are also due to the interplay between these systems and are driven directly by this process. Perfectly consistent wind-stress computations would require an atmosphere-ocean-wave coupled system. Even in such a situation, the wave-informed drag ultimately depends on the ability of the wave model to represent the tail of the wave spectrum (growing short waves), which is in itself challenging and carries great uncertainty. For numerical reasons, the equations in the wave models are often only integrated up to a cut-off prognostic frequency and the tail is diagnosed assuming a certain shape (Bidlot, 2012) . Besides, the spectrum will depend on the chosen wave generation/growth and dissipation parameterizations as well. Given all these sources of uncertainty, it is not surprising that the accurate and consistent computation of the wave induced drag and ultimately the sea-surface roughness remains a challenging topic in the research community. Beyond the effects of the sea-state dependent roughness, the other two considered coupling components are also parameterized differently in 2DH and 3D systems. The Stokes-Coriolis drift presents a vertical velocity profile which is parameterized in CMEMS (Breivik et al., 2016) but not accounted for in depth averaged models such as ANYEU-SSL. The effect of this drift is strongly localized at the surface of the ocean. Furthermore, wave-breaking induced turbulent kinetic energy fluxes are again simply not represented in 2DH models. While reported to be of second order compared to the momentum flux effects, these coupling processes have shown to have in the present

work and in literature a non-negligible impact on WLs. Finally, it is noteworthy that reported significant tidal modulations of the nearshore wave height will be partially absent in the CMEMS operational models (including the IBI model) due to the fact that only tidal currents and not levels are currently being coupled (except for the Mediterranean and Black Sea models, where this effect is expected to be small given their micro-tidal regime), while both are transmitted in the ANYEU-SSL model. Eventually, the resolution of the models is potentially too coarse to fully resolve this process (Lewis et al., 2019).

The limitations of the current study include the short period being analyzed (1-year), for which only a handful of extreme events can be assessed, as well as the lack of assessment of the resulting ocean-coupled wave fields. These were not the main focus of the study, but they will indirectly contribute to coastal TWLs in ECFAS via the wave setup, formulated as a function of the modelled offshore significant wave height. At a qualitative level, the two systems show a similar spatial distribution of the errors during extremes, with generally underpredicted extreme surges and with largest errors around the German Bight. This is presumably affected by the lack of wetting and drying in both models, and the associated measure of capping the depth above the local lowest tide levels.

6 Feedbacks for the ECFAS roadmap

As stated in section 1.2, the experiments performed in the present work and the analysis therein have the ultimate objective of identifying the technical requirements of the marine modelling tools employed for coastal TWL forecasting within coastal flood risk applications, and in particular for the ECFAS proof-of-concept and its future evolutions. Therefore, the implication of the present results for ECFAS are discussed explicitly and will inform the ECFAS roadmap (**D6.4 - Roadmap of ECFAS integration into CEMS).**

First, the production of the hindcast is addressed. As reported in **D4.1 – Report on the calibration and validation of hindcasts and forecasts of TWL**, the hindcast was produced by a linear addition of surges (as computed by ANYEU-SSL) and an external source for tides, and therefore tide-surge interactions were not accounted for. As demonstrated in section 3.1.1., this can lead to an underestimation/overestimation of the coastal extreme surges. Additionally, it has been observed in the present work and confirmed by the literature that such non-linear interaction can lead to a difference in timing between the peak surges and peak tides, resulting in reduced/increased WL extremes compared to the linear approach. These interaction effects will have implications for the derivation of historical thresholds for extremes (**D4.3 - Report on the identification of local thresholds of TWL for triggering coastal flooding**) and will therefore directly impact the performance of the triggering of the warning system. In fact, the historical extreme values are also used to produce the flood catalogue (**D5.4 -Pan-EU flood maps catalogue**), which will therefore inevitably inherit these biases. Furthermore, wave-coupling was not accounted for in the production of the hindcast. The implications are equivalent to those described for the lack of tide-surge interaction, with the added layer of complexity given by the fact that the interaction is in reality 3-way (tide-surge-wave). Beyond the implications from the linear method used to compose the historical water-levels (hindcast), given its 2DH nature, the ANYEU-SSL model simply lacks the capability to accommodate some of the evaluated physical processes such as the impact of wave-breaking induced mixing, and effects such as the observed impact of the wave-coupling on baroclinic motions in CMEMS-IBI (section c.3.23.2.1). Furthermore, the current bathymetry capping at a minimum of 10 meters in ANYEU-SSL (**D4.1 – Report on the calibration and validation of hindcasts and forecasts of TWL**) is expected to limit the capability of the model to represent coastal water-levels and non-linear interactions in wide shallow regions such as the southern North Sea, as was depicted in Figure 4.1. It is recommended that both hindcast and forecast models employed in

the future should avoid the use of capped depths, which implies the numerical implementation of wetting and drying. It is expected that such a development would greatly increase the coastal capabilities of the models in areas such as the Northwest Shelf.

Second, the current configuration of the CMEMS models used for the operational forecasts is addressed. As described in **D4.1 – Report on the calibration and validation of hindcasts and forecasts of TWL**, all ocean models currently account for explicit representation of tides, therefore allowing for tide-surge interaction, except for the Black Sea where the interaction is expected to be negligible. However, it was also shown that the ocean models account for varying levels of wave-coupling, the IBI regional model being the only one accounting for all processes as described in the present work (section 2). For example, the NWS model does not account for variable wave-induced breaking energy flux, while it has been seen in this study and literature that non-negligible effects can be seen in the shallow southern North Sea and several estuaries. It is therefore recommended, for the present application, that all models employ their full wave-coupling capabilities in future evolutions. In addition, it is highlighted that currently an inconsistency exists in the computation of the wind stress between the atmospheric model forcing the models, the ocean models, and the wave models. Since the 3 components are not fully coupled in the CMEMS systems, 100% consistency cannot be achieved in this regard, but steps can be taken to increase it. As argued in section 5, the meteorological winds at 10-meters could be used together with the roughness (Charnock) computed by the atmospheric model in order to obtain more consistent wind stresses to force the ocean and wave models. Given the inevitable mismatch between the wave model underlying the atmospheric model and the wave model at hand, iterative schemes could be explored to converge on the roughness field. Besides, the information on the stability of the atmospheric boundary layer could be shared from the ocean to the wave models, which can have a considerable effect on the effective wind drag as shown by Clementi et al. (2018). At least, experimental studies addressing these inconsistencies would inform on the associated uncertainties, interlinkages, and best approach to tackle them for off-line coupled systems such as the ones in CMEMS and hence ECFAS. Given the driving role of the wind stress on storm surges, it is believed that this aspect is of great importance for the ECFAS system. Furthermore, it is highlighted that water-levels are not coupled in any of the ocean-wave systems in CMEMS for the meso- and macro-tidal environments, while known to locally modulate the wave-fields in such environments as discussed in section5. This aspect could impact the computation of the wave-setup, which in the current prototype of ECFAS relies on

the significant wave height for both the hindcast and the forecasts. It is therefore recommended that this additional coupling is considered in future versions of the CMEMS systems, especially on those regions with strong tidal dynamics (IBI, NWS).

Finally, the consistency between the produced hindcast and the operational forecasts of TWL is addressed from the perspective of their current model complexity and associated impacts. The important differences in the type and nature of the physical processes included, as described above, may lead to important biases in the magnitude and frequency of extreme events. While this may be partly accounted for through simplistic bias correction methods (**T4.5 - Identification of thresholds for triggering coastal flood mapping**), the complex spatio-temporal nature of the expected biases will remain partly unaccounted for and difficult to quantify. This may have important implications at the interface between the two datasets, namely at the triggering step of the ECFAS workflow. In an ideal setup, the hindcast and forecasts would be produced by the same modelling systems, or at least same type of modelling systems. In this regard, the CMEMS models provide a more complete (and in principle realistic) characterization of the water-levels given their added complexity compared to the ANYEU(-SSL) system and data assimilation. On the other hand, using lighter 2DH models such as ANYEU-SSL facilitates the production of long hindcasts (important for the determination of thresholds, **T4.5 - Identification of thresholds for triggering coastal flood mapping**) as well as interesting techniques for operational forecasting such as ensemble forecasting, which would result considerably more computationally expensive for 3D models. Such techniques could help better account for forecast uncertainties. The lack of baroclinic processes, which are important in the determination of extremes in areas like the Mediterranean, could be accounted for through the combination with external sea-level datasets as was done in the production of the combined hindcasts in **D4.1 – Report on the calibration and validation of hindcasts and forecasts of TWL,** while inevitably missing certain non-linear feedbacks**.** All in all, increased coherence between the hindcast and forecasts is recommended in future evolutions of the ECFAS system.

7 Summary and Conclusions

In the present work, the influence of increased model complexity in the representation of coastal (extreme) water-levels has been evaluated through the analysis of a number of numerical experiments in which complexity is increased by gradually adding physical processes that have been reported in literature to influence water-levels. Additionally, such experiments have been performed on 2 modelling systems with depth-averaged (2-dimensional, 2DH) and 3-dimensional (3D) configurations (both type of systems found to be used in literature for coastal TWL forecasting), in order to evaluate the sensitivity of each type of configuration to the evaluated processes. The objective of such exercise is to identify the requirements needed for modelling systems that target coastal water-levels typically used for coastal flood risk applications and provide recommendations for future possible evolutions of the warning component of the ECFAS system. The modelling systems employed are those used within the ECFAS prototype for the production of TWL hindcasts and forecasts and evaluated in **D4.1 – Report on the calibration and validation of hindcasts and forecasts of TWL**, that is, the ANYEU-SSL European model (2DH) and the CMEMS ocean model (3D). For the latter, the IBI configuration is used only (CMEMS-IBI), for a former release version of the operational system, covering in its native configuration the IBI and the NWS regions as defined in CMEMS. The experiments are performed for the year 2018, where a number of known important storm events took place (storms Eleanor, Emma, Vaia). These events are included in the list of events used in the validation activities within ECFAS (**D5.1 – Database of extreme events, test cases selection and available data**, **D5.2 – Validated LISFLOOD-FP model for coastal areas**, **D4.1 – Report on the calibration and validation of hindcasts and forecasts of TWL**).

The models are evaluated for the following processes: tide-surge non-linear interaction, which is evaluated only with the ANYEU-SSL model, and the interactions influence of waves on the water-levels, which is evaluated in both systems through coupling with their respective wave model. The results focus on the impacts on the non-tidal residual (NTR) due to the expected main impact on this component (given the dominating gravitational nature of tides) and in order to increase the sample of storm-driven extreme events within 2018, while for the tide-surge interaction assessment impacts on tidal propagation are also shown. The evaluation of tide-surge interaction shows a clear impact of this process under average and more importantly under extreme conditions, mostly concentrated around the Northwest Shelf, where both increase and decrease of extreme values by several decimetres up to a metre are

observed, matching reported magnitudes in literature. This interaction is confirmed to play a crucial role on the accurate determination of coastal WL extremes (magnitude and timing) for a large part of the European coasts and is hence deemed essential in applications such as ECFAS. In contrast, the wave-coupling effects show a moderate to small influence for both average and extreme conditions when evaluated in the ANYEU-SSL system (2DH). A mild increase in surge extremes is seen for the northern European coasts (max +14%/+9 cm in the German Bight) while a more substantial decrease is seen for the southern European coasts (min -25%, eastern Mediterranean). When evaluated in the CMEMS-IBI model (3D), however, the impact appears significantly larger and especially so during extreme events (max +28% in the German Bight), with extreme surges typically growing and with largest impacts in the order of several decimetres (+40 cm during storm Eleanor at the Dutch coast) and concentrated on the Northwest Shelf. The main driver appears to be the wave-dependent sea surface roughness, with the Stokes-Coriolis drift and wave-breaking induced mixing being of second order and mostly limited to off-the-shelf regions (mesoscale dynamics) and some isolated estuarine areas (German Bight). The magnitudes and spatial distribution of impacts seen for CMEMS-IBI for each component are in good agreement with literature. A plausible reason for the too-low sensitivity of the ANYEU-SSL to wave coupling and in particular to the wave-dependent sea roughness could be a positive bias in the default sea-roughness parameterization in non-coupled conditions, entailing that wave-coupling either very marginally increases the resulting roughness or even significantly reduces it, as is the case across southern European coasts. Notably, the inclusion of wave-coupling processes substantially improved the performance during extreme events for the CMEMS-IBI system (and also but less substantially for the ANYEU-SSL model), especially around the North Sea where the original underprediction was largest. Mean peak magnitude errors for both WLs and surges nearly halve for the CMEMS-IBI system, while they reduce by up to 10 cm for the ANYEU-SSL system around the German Bight area.

Based on these results, and given the characteristics and approach followed for the production of hindcasts and forecasts (marine forcing) described in **D4.1 – Report on the calibration and validation of hindcasts and forecasts of TWL**, the following recommendations are made for the future evolutions of the marine forcing component of the ECFAS system. Accounting for the tide-surge interactions as well as wave-surge interactions is encouraged to increase the accuracy of coastal TWLs forecasts and hindcasts (**D4.1 – Report on the calibration and validation of hindcasts and forecasts of TWL)**, entailing a major change on the approach

followed for the hindcast production in the current ECFAS prototype where both these processes are currently missing. The generated potential biases in historical extreme water-levels will inevitably impact the downstream flood magnitudes and their recurrence. For the CMEMS models providing the forecasts to the system, homogenization of the wave-coupling components to a fully coupled setup is recommended for all regions, which currently account for this process at varying degrees. Additionally, the addition of water-level coupling into the wave models is recommended for tidally energetic regions as currently only currents are coupled in the CMEMS models. It is noteworthy that adding levels of complexity to models comes at a cost: increasing the volume of data and CPU time, which have to be considered for operational systems. Finally, it is stressed that an increase in coherence between hindcasts and forecasts would greatly increase the reliability and consistency of the marine forcing warnings, on which the whole ECFAS workflow relies for activation.

8 Acknowledgements

The authors thank Gabriel Moutappa who contributed to the present work through the development of the scripts for the intra-model comparisons for the CMEMS-IBI model. The authors also thank Météo France who provided the simulation outputs of the experiments for the CMEMS-IBI system. Additionally, the authors thank Malek Ghantous (CLS, previously Météo France) who performed the simulation experiments for the CMEMS-IBI system and offered his expertise in the use and interpretation of the simulation outputs. Finally, the authors thank Stéphane Law Chune for his expert advice in the understanding of the wave-coupling processes and their numerical implementation, as well as in the interpretation of the present results.

9 References

Aouf, L., & Lefèvre, J. M. (2015). On the impact of the assimilation of SARAL/AltiKa wave data in the operational wave model MFWAM. *Marine Geodesy*, *38*(sup1), 381-395.

Arns, A., Wahl, T., Dangendorf, S., & Jensen, J. (2015). The impact of sea level rise on storm surge water levels in the northern part of the German Bight. *Coastal Engineering*, *96*, 118–131. https://doi.org/10.1016/j.coastaleng.2014.12.002

Bertin, X., Li, K., Roland, A., & Bidlot, J.-R. (2015). The contribution of short-waves in storm surges: Two case studies in the Bay of Biscay. *Continental Shelf Research*, *96*, 1–15. https://doi.org/10.1016/j.csr.2015.01.005

Bidlot, J.-R. (2012). *Present status of wave forecasting at ECMWF.*

Bonaduce, A., Staneva, J., Grayek, S., Bidlot, J.-R., & Breivik, Ø. (2020). Sea-state contributions to sea-level variability in the European Seas. *Ocean Dynamics*, *70*(12), 1547–1569. https://doi.org/10.1007/s10236-020-01404-1

Breivik, Ø., Bidlot, J.-R., & Janssen, P. A. E. M. (2016). A Stokes drift approximation based on the Phillips spectrum. *Ocean Modelling*, *100*, 49–56. https://doi.org/10.1016/j.ocemod.2016.01.005

Clementi, E., Oddo, P., Drudi, M., Pinardi, N., Korres, G., & Grandi, A. (2017). Coupling hydrodynamic and wave models: first step and sensitivity experiments in the Mediterranean Sea. *Ocean Dynamics*, *67*(10), 1293–1312. https://doi.org/10.1007/s10236-017-1087-7

Codiga, D. (2011). *Unified tidal analysis and prediction using the UTide Matlab functions*. Graduate School of Oceanography, University of Rhode Island, Narragansett,.

Fernández-Montblanc, T., Vousdoukas, M. I., Ciavola, P., Voukouvalas, E., Mentaschi, L., Breyiannis, G., Feyen, L., & Salamon, P. (2019). Towards robust pan-European storm surge forecasting. *Ocean Modelling*, *133*, 129–144. https://doi.org/10.1016/j.ocemod.2018.12.001

Fernández-Montblanc, T., Vousdoukas, M. I., Mentaschi, L., & Ciavola, P. (2020). A Pan-European high resolution storm surge hindcast. *Environment International*, *135*, 105367. https://doi.org/10.1016/j.envint.2019.105367

Hersbach, H., Bell, B., Berrisford, P., Hirahara, S., Horányi, A., Muñoz-Sabater, J., Nicolas, J., Peubey, C., Radu, R., Schepers, D., Simmons, A., Soci, C., Abdalla, S., Abellan, X., Balsamo, G., Bechtold, P., Biavati, G., Bidlot, J., Bonavita, M., Thépaut, J. (2020). The ERA5 global reanalysis. *Quarterly Journal of the Royal Meteorological Society*, *146*(730), 1999–2049. https://doi.org/10.1002/qj.3803

Horsburgh, K. J., & Wilson, C. (2007). Tide-surge interaction and its role in the distribution of surge residuals in the North Sea. *Journal of Geophysical Research*, *112*(C8), C08003. https://doi.org/10.1029/2006JC004033

Hsu, T.-W., Ou, S.-H., & Liau, J.-M. (2005). Hindcasting nearshore wind waves using a FEM code for SWAN. *Coastal Engineering*, *52*(2), 177–195. https://doi.org/10.1016/j.coastaleng.2004.11.005

Idier, D., Bertin, X., Thompson, P., & Pickering, M. D. (2019). Interactions Between Mean Sea Level, Tide, Surge, Waves and Flooding: Mechanisms and Contributions to Sea Level Variations at the Coast. *Surveys in Geophysics*, *40*(6), 1603–1630. https://doi.org/10.1007/s10712-019-09549-5

Idier, D., Dumas, F., & Muller, H. (2012). Tide-surge interaction in the English Channel. *Natural Hazards and Earth System Sciences*, *12*(12), 3709–3718. https://doi.org/10.5194/nhess-12-3709-2012

Law Chune, S., & Aouf, L. (2018). Wave effects in global ocean modeling: parametrizations vs. forcing from a wave model. *Ocean Dynamics*, *68*(12), 1739–1758. https://doi.org/10.1007/s10236-018-1220-2

Lewis, M. J., Palmer, T., Hashemi, R., Robins, P., Saulter, A., Brown, J., Lewis, H., & Neill, S. (2019). Wave-tide interaction modulates nearshore wave height. *Ocean Dynamics*, *69*(3), 367–384. https://doi.org/10.1007/s10236-018-01245-z

Lyard, F. H., Allain, D. J., Cancet, M., Carrère, L., & Picot, N. (2021). FES2014 global ocean tide atlas: design and performance. *Ocean Science*, *17*(3), 615–649. https://doi.org/10.5194/os-17-615-2021

Madec, G., Bourdallé-Badie, R., Bouttier, P. A., Bricaud, C., Bruciaferri, D., Calvert, D., ... & Vancoppenolle, M. (2017). NEMO ocean engine.

Pineau-Guillou, L., Ardhuin, F., Bouin, M., Redelsperger, J., Chapron, B., Bidlot, J., & Quilfen, Y. (2018). Strong winds in a coupled wave–atmosphere model during a North Atlantic storm event: evaluation against observations. *Quarterly Journal of the Royal Meteorological Society*, *144*(711), 317–332. https://doi.org/10.1002/qj.3205

Pineau-Guillou, L., Bouin, M.-N., Ardhuin, F., Lyard, F., Bidlot, J.-R., & Chapron, B. (2020). Impact of wave-dependent stress on storm surge simulations in the North Sea: Ocean model evaluation against in situ and satellite observations. *Ocean Modelling*, *154*, 101694. https://doi.org/10.1016/j.ocemod.2020.101694

Pond, S., & Pickard., G. (1983). *Introductory dynamical oceanography.* Gulf Professional Publishing.

Roland, A., Zhang, Y. J., Wang, H. v., Meng, Y., Teng, Y.-C., Maderich, V., Brovchenko, I., Dutour-Sikiric, M., & Zanke, U. (2012). A fully coupled 3D wave-current interaction model on

unstructured grids. *Journal of Geophysical Research: Oceans*, *117*(C11), n/a-n/a. https://doi.org/10.1029/2012JC007952

Smith, S. D., & Banke, E. G. (1975). Variation of the sea surface drag coefficient with wind speed. *Quarterly Journal of the Royal Meteorological Society*, *101*(429), 665–673. https://doi.org/10.1002/qj.49710142920

Staneva, J., Alari, V., Breivik, Ø., Bidlot, J.-R., & Mogensen, K. (2017). Effects of wave-induced forcing on a circulation model of the North Sea. *Ocean Dynamics*, *67*(1), 81–101. https://doi.org/10.1007/s10236-016-1009-0

Staneva, J., Wahle, K., Koch, W., Behrens, A., Fenoglio-Marc, L., & Stanev, E. v. (2016). Coastal flooding: impact of waves on storm surge during extremes – a case study for the German Bight. *Natural Hazards and Earth System Sciences*, *16*(11), 2373–2389. https://doi.org/10.5194/nhess-16-2373-2016

Wolf, J. (2009). Coastal flooding: impacts of coupled wave–surge–tide models. *Natural Hazards*, *49*(2), 241–260. https://doi.org/10.1007/s11069-008-9316-5

Woodworth, P. L., Melet, A., Marcos, M., Ray, R. D., Wöppelmann, G., Sasaki, Y. N., ... & Merrifield, M. A. (2019). Forcing factors affecting sea level changes at the coast. *Surveys in Geophysics*, *40*(6), 1351-1397.

Zhang, Y., & Baptista, A. M. (2008). SELFE: A semi-implicit Eulerian–Lagrangian finite-element model for cross-scale ocean circulation. *Ocean Modelling*, *21*(3–4), 71–96. https://doi.org/10.1016/j.ocemod.2007.11.005

Zijl, F., Verlaan, M., & Gerritsen, H. (2013). Improved water-level forecasting for the Northwest European Shelf and North Sea through direct modelling of tide, surge and non-linear interaction. *Ocean Dynamics*, *63*(7), 823–847. https://doi.org/10.1007/s10236-013-0624-2